Synthesis, Characterization, and Study of Photoinduced Optical Anisotropy in Polyimides Containing Side Azobenzene Units

Ewa Schab-Balcerzak,*,† Mariola Siwy,† Michal Kawalec,† Anna Sobolewska,‡ Agata Chamera,‡ and Andrzej Miniewicz‡

Centre of Polymer and Carbon Materials, Polish Academy of Sciences, M. Curie-Sklodowska 34, 41-819 Zabrze, Poland, and Institute of Physical and Theoretical Chemistry, Wroclaw University of Technology, Wybrzeze Wyspianskiego 27, 50-370 Wroclaw, Poland

Received: May 7, 2009; Revised Manuscript Received: June 19, 2009

In this paper, novel processable aromatic polymers with imide rings and attached as side-chain azobenzene units are presented. Polymers differ in the chemical structures of chromophores and polymer backbones. Azopolymers were obtained by a two-step synthetic approach. This includes the preparation of a precursor poly(esterimide) and poly(etherimide) with pendant phenolic hydroxyl groups, followed by the covalent bonding of NLO chromophores onto the polyimide backbone by the Mitsunobu reaction. The degree of functionalization of polymers was estimated by UV−vis spectroscopy. Polymers were characterized and evaluated by FT-IR, ^{1}H NMR, X-ray, UV−vis, DSC, and TGA methods. The synthesized polymers exhibited glass transition temperatures in the range of 167−228 °C, thermal stability with decomposition temperatures in the range of 275−446 °C, and excellent solubilities in common organic solvents. The light-induced optical anisotropy was studied in obtained azopolymers with the help of a holographic grating recording technique. Two polarization geometries were applied for the grating inscription s−s and p−p. The influence of the polarization geometry on the diffraction efficiency dynamics and on the depth of the surface modulation was not observed, which is different from results reported in the literature. Surface relief gratings, which appeared after the light exposure, were observed by atomic force microscopy. Additionally, the optical anisotropy in poly(esterimide)s was investigated by photoinduced birefringence measurements. For the first time, in polyimide with covalently bonded azobenzene derivatives, the high photoinduced birefringence ($\Delta n = 0.01$) was measured.

Introduction

There is an increasing interest in studying photonic processes, allowing for the improvement of optical devices for storage, processing, displaying, and transfer of information. The phenomenon of photoinduced optical anisotropy (POA) is a key for this purpose.[1] The challenging issue is the choice and preparation of suitable optical and NLO materials. The use of polymers for photonic and optoelectronic applications offers many advantages in comparison with inorganic materials, for example, the great flexibility of polymer−chromophore combinations that can be selected to suit particular applications. Various NLO polymers are currently synthesized and studied by a large number of research groups. However, for the generation of photoinduced optical anisotropy with the unique possibility of mapping polarization states of incoming light, azobenzene-containing polymers are considered as the most effective materials.[2] Azobenzene groups are known to exist in two isomeric states, a thermodynamically stable trans and a metastable cis form. When irradiated with light of an appropriate wavelength, they undergo a multiple reversible trans ↔ cis photoisomerization process.[3] For random distribution of the azobenzene groups in a viscous polymeric matrix, a linearly polarized laser light causes the orientation of the azobenzene moieties perpendicular to the electric field vector of the incident light, which results in the induction of the optical anisotropy. In azo-dye-functionalized polymeric films, photoisomerization induces an orientation of dyes at room temperature, that is, far below the respective polymer glass transition temperature, where the spontaneous movements of polymer segments are essentially frozen.[4] The most convenient method of using azobenzene chromophores, from a practical point of view, is incorporating them into polymers as fully covalent bonded structure elements in the main or side chain of the polymer macromolecule.[5] It is obvious that the efficiency and stability of the photoinduced optical anisotropy in such polymers will strongly depend on the chromophore architecture, the structure of the macromolecules facilitating or hindering the chromophore mobility, and also molecular near-neighbor interactions of photochromic units with the polymer chain.

The most frequently studied types of azobenzene-based materials are acrylate and methacrylate polymers and their copolymers.[6,7] Other polymers such as polyurethanes,[8,9] epoxy-based polymers,[10−13] polyesters,[14] polyureas,[15] and polyimides[16] are also investigated. Polyimides play a key role as materials for many applications ranging from dielectric films for the electronics industry and orientation layers liquid crystal industry, to lightweight load-bearing heat-resistant composites and adhesives for the aerospace industry, to gas separation membranes due to their outstanding thermal, mechanical, electrical, and chemical resistance properties.[17,18] Such performances have inspired many researchers to modify, study, and utilize polyimides in the field of optoelectronics, namely, with respect to their second-order NLO phenomena.[19−23] To the best of our knowledge, apart from our research group, only in a few articles

* To whom correspondence should be addressed. E-mail: eschab-balcerzak@cmpw-pan.edu.pl.
† Polish Academy of Sciences.
‡ Wroclaw University of Technology.

10.1021/jp904250r CCC: $40.75
Published on Web 07/08/2009

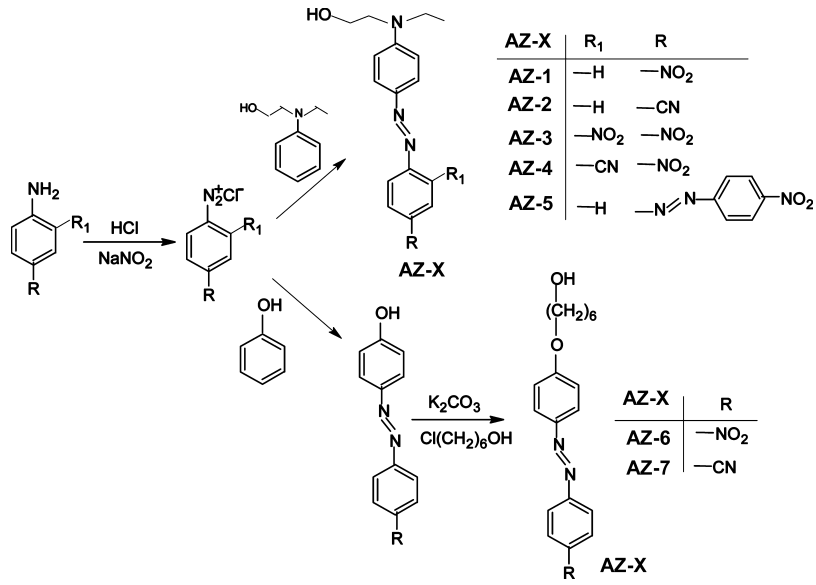

Figure 1. Chemical structures and synthesis of azobenzene chromophores **AZ-X.**

TABLE 1: Calculated Dipole Moments (μ) and Position of the Absorption Maximum (λ_{max}) for Chromophores AZ-X

AZ-X	AZ-1	AZ-2	AZ-3	AZ-4	AZ-5	AZ-6	AZ-7
μ^a [D]	8.39	8.32	9.02	9.39	9.54	6.92	6.17
λ_{max} [nm]	500	479	532	548	532	383	371

[a] Calculated with the James J. P. Stewart's MOPAC2007 8.032W program.

were third-order NLO properties suitable for optical data storage investigated.[24−28]

In the past decades, several synthetic routes for side-chain NLO azopolyimides have been developed. Most of them were synthesized via a general condensation reaction between diamines and dianhydrides to afford poly(amic acid) precursor polymers, followed by a high-temperature imidization or a chemical imidiaztion process to produce the projected polyimides. The relatively harsh chemical conditions of the monomer synthesis and the imidiaztion process can be dangerous for chromophores. Another facile approach for the synthesis of chromophore-functionalized polyimides is a mild postfunctionalization reaction. This strategy can be realized in two different manners. The first one uses the azo coupling reaction, which is the commonly used method for azo-dye synthesis and was first reported by Liu et al.[29] The second one includes the preparation of the hydroxyl-containing polyimide followed by the covalent bonding of NLO chromophores into the polyimide backbone via a Mitsunobu condensation.[30,31] The latter method was applied for the preparation of the polymers presented in this article. In these polymers, azochromophores were connected by flexible tethers to main chains of the polyimide-containing ester or ethers groups. Two kinds of chromophores with nitro and/or cyano groups were applied. One of them based the nitro and/or cyano group connected with the azobenzene group as the acceptor end of a donor−π-bridge acceptor and a hydroxyl functional amino group as the donor end, that is, DR1-type chromophores. The second one also possesses the nitro and/or cyano group but did not contain the amino group in the linkage between azobenzene and the polymer backbone. Second-order NLO phenomena have already been investigated in polyimides containing flexibly tethered DR1 chromophoric side groups,[30,31] whereas the light-induced orientation in such a type of polymers has been reported only by measurements of photoinduced dichroism.[24]

This paper reports the synthesis and characterization of novel NLO side-chain-modified aromatic polyimides as well as the investigation of the light-induced optical anisotropy in these polymers. POA was studied by measurements of the photoinduced birefringence and the holographic diffraction grating recording.

Experimental Section

Materials. Diethylazodicarboxylate (DEAD), triphenylphosphine, 2,4-diaminophenol dihydrochloride, 6-chloro-1-hexanol, 2-cyan-4-nitroaniline, 4-cyanoaniline, *p*-nitroaniline, Disperse Orange 3, 2-(*N*-ethylanilino)ethanol, phenol,4,4′-(4,4′-isopropylidene diphenoxy)bis(phthalic anhydride), Disperse Red 1 (denoted as chromophore **AZ-1**), and *N*-methyl-2-pyrrolidone (NMP) were purchased from Aldrich Chemical Co. and were used without purification. Chromophore 4-[4-(6-hydroxyhexyloxy)phenylazo]benzonitrile (**AZ-7**) was synthesized according to the procedure published elsewhere.[32,33] 4,4′[Diphenylopropane-di(benzene-5-estro-1,2-dicarboxylic)]anhydride was prepared as reported in our previous paper.[34]

Synthesis of Chromophores AZ-2 to AZ-6. AZ-2 (*N*-ethyl-*N*-(2-hydroxylethyl)-4-(4-cyanophenylazo)aniline) was synthesized according to the published procedure.[35] **AZ-2**: ^{1}H NMR (DMSO-d_6, δ, ppm): 1.14 (t, CH_3, 3H), 3.51 (t, CH_2, 2H), 3.54 (t, CH_2, 2H), 3.59 (q, CH_2, 2H), 4.84 (t, OH, H), 6.85 (d, 2H), 7.79 (d, 2H), 7.85 (d, 2H), 7.96 (d, 2H). FTIR (KBr, cm^{-1}): 3489 (OH), 2968, 2945 (CH_2), 2229 (CN). UV−vis (NMP): λ_{max} = 280 and 479 nm, $\varepsilon_{479} = 3.17 \times 10^4$ [L/mol cm], mp = 138 °C. Yield: 90%.

AZ-3 (*N*-ethyl-*N*-(2-hydroxylethyl)-4-(2,4-dinitrophenylazo)aniline) was prepared according to the modified method.[7] A solution of hydrochloric acid (36%, 1.4 mL) was added to 2,4-dinitroaniline (0.916 g, 5 mmol), and the mixture was stirred and heated to 60−70 °C. Into the resulting warm solution, 10 mL of water and 15 mL of acetic acid (99.5%) were added. The reaction mixture was stirred overnight. Then, 10 mL of acetic acid was added, and the reaction mixture was stirred again

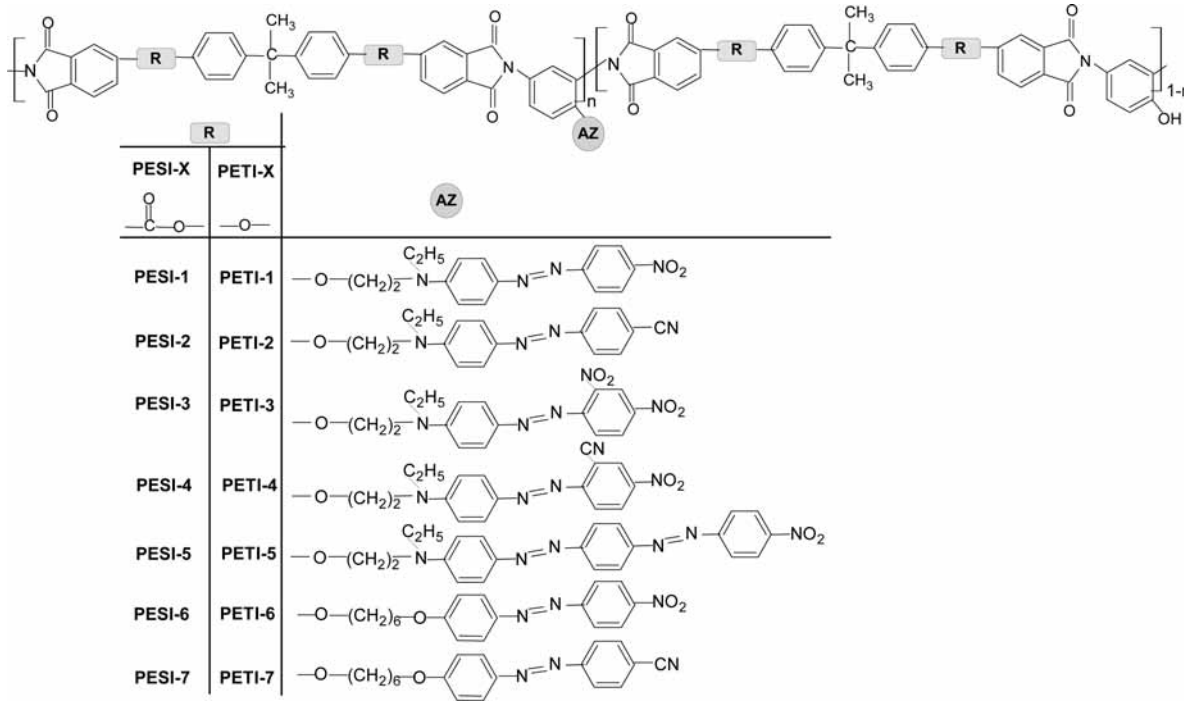

Figure 2. Chemical structures of synthesized azobenzene functionalized polymers **PESI-X** and **PETI-X**.

TABLE 2: The Chromophore Loading Level in Studied Polymers and the Polymer Solubility[a]

		solubility				
	chromophore loading level	THF	$CHCl_3$		CH_3CN	
polymer code	[%]	20 °C	20 °C	50 °C	20 °C	50 °C
PESI-OH	0	+	±	±	−	−
PESI-1	81	+	+	+	±	±
PESI-1a	10	+	+	+	±	±
PESI-2	23	+	±	±	±	±
PESI-3	40	+	±	±	±	±
PESI-4	69	+	±	±	±	±
PESI-5	47	+	±	±	±	±
PESI-6	55	+	+	+	±	±
PESI-7	75	+	+	+	±	±
PETI-OH	0	+	±	±	−	−
PETI-1	33	+	±	±	±	±
PETI-1a	5	+	±	±	−	−
PETI-2	77	+	+	+	±	±
PETI-3	43	+	±	±	±	±
PETI-4	61	+	±	±	±	±
PETI-5	−	−	−	−	−	−
PETI-6	36	+	±	±	−	±
PETI-7	83	+	±	±	−	±

[a] Symbols: + soluble; ± partially soluble; − insoluble.

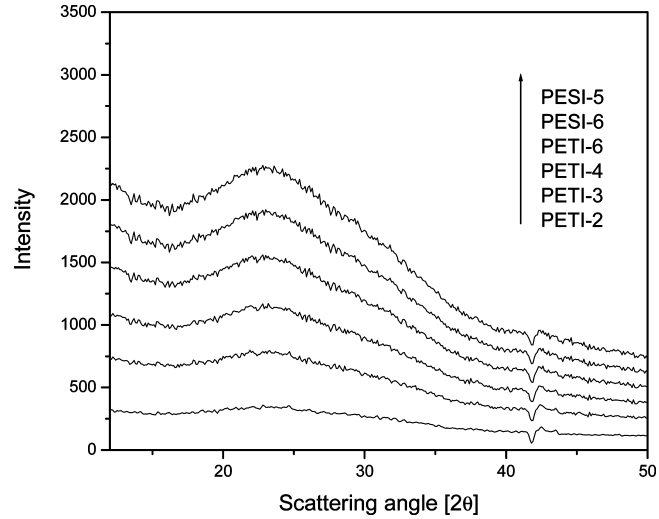

Figure 3. X-ray diffraction patterns of the prepared azopolymers **PESI-5**, **PESI-6**, **PETI-2**-**PETI-4**, and **PETI-6**.

overnight. Afterward, the flask was cooled down to 0−5 °C in the ice bath, and the solution of sodium nitrite (0.4 g, 6 mmol) in 1 mL of water was added dropwise under stirring. After stirring for 3 h, to the diazonium salt solution, 2-(*N*-ethylanilino)ethanol (0.909 g, 5.5 mmol) dissolved in 2 mL of methanol was added dropwise, and the mixture was stirred for 0.5 h under cooling, followed by neutralization (pH 5−6) with anhydrous sodium acetate (10 g, 120 mmol). It was stirred for 1 h more, and the reaction mixture was kept overnight in a refrigerator. Then, the solution was poured into water, and the precipitate formed was collected, washed with plenty of water and methanol, and dried. **AZ-3**: ^{1}H NMR (DMSO-d_6, δ, ppm): 1.16 (t, CH_3, 3H), 3.53 (t, CH_2, 2H), 3.56 (t, CH_2, 2H), 3.61 (q, CH_2, 2H), 4.86 (t, OH, H), 6.90 (d, 2H), 7.70 (d, 2H), 7.82 (d, H), 8.23 (q, H), 8.41 (d, H). FTIR (KBr, cm^{-1}): 3089 (OH), 2972, 2918 (CH_2), 1516, 1347 (NO_2). UV−vis (NMP): λ_{max} = 292 and 532 nm, $\varepsilon_{532} = 5.152 \times 10^4$ [L/mol cm], mp = 132 °C. Yield: 40%.

AZ-4 (*N*-ethyl-*N*-(2-hydroxylethyl)-4-(2-cyano-4-nitrophenylazo)aniline) was prepared from 2-cyan-4-nitroaniline via the same procedure as described for the synthesis of **AZ-3**. **AZ-4**: ^{1}H NMR (DMSO-d_6, δ, ppm): 1.17 (t, CH_3, 3H), 3.56 (t, CH_2, 2H), 3.58 (t, CH_2, 2H), 3.62 (q, CH_2, 2H), 4.90 (t, OH, H), 6.83 (d, 2H), 7.84 (d, 2H), 7.88 (d, H), 8.10 (q, H), 8.45 (d, H). FTIR (KBr, cm^{-1}): 3334 (OH), 2952, 2903 (CH_2), 2230 (CN), 1509, 1324 (NO_2). UV−vis (NMP): λ_{max} = 364, 548 nm, $\varepsilon = 1.12 \times 10^4$ [L/mol cm], mp = 136 °C. Yield: 41%.

AZ-5 (4-nitro-4′(*N*-ethyl-*N*-(2-hydroxylethyl)) amino-bisazobenzene) was synthesized according to the published procedure.[34] **AZ-5**: ^{1}H NMR (DMSO-d_6, δ, ppm): 1.15 (t, CH_3, 3H), 3.50 (t, CH_2, 2H), 3.53 (t, CH_2, 2H), 3.61 (q, CH_2, 2H), 4.80 (t,

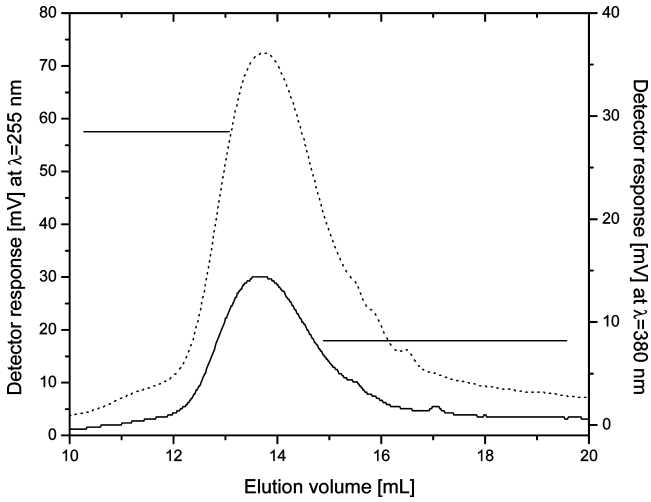

Figure 4. Overlay plot of SEC elugrams of the polymer **PETI-7** obtained with UV detector at wavelengths of 255 (dotted line) and 380 nm (solid line).

OH, H), 6.86 (d, 2H), 7.95−8.12 (m, 6H), 8.44 (d, 2H). FTIR (KBr, cm^{-1}): 3103 (OH), 2929, 2965 (CH_2), 1516, 1342 (NO_2). UV−vis (NMP): $\lambda_{max} = 532$ nm, $\varepsilon = 2.674 \times 10^4$ [L/mol cm], mp = 219 °C. Yield: 70%.

AZ-6 (4-[4-(6-hydroxyhexyloxy)phenylazo]nitrobenzene) was synthesized according to the procedure described elsewhere.[32,33] **AZ-6**: ^{1}H NMR (DMSO-d_6, δ, ppm): 1.36−1.46 (m, CH_2, 4H), 1.72−1.74 (m, CH_2, 4H), 4.07−4.12 (m, CH_2, 4H), 4.35 (t, OH, H), 7.16 (d, 2H), 7.96 (d, 2H), 8.03 (d, 2H), 8.42 (d, 2H). FTIR (KBr, cm^{-1}): 3557 (OH), 2909, 2868 (CH_2). UV−vis (NMP): $\lambda_{max} = 383$ nm, $\varepsilon_{383} = 4.53 \times 10^4$ [L/mol cm], mp = 131 °C. Yield: 41%.

Synthesis of Polymers. The synthesis and characterization of hydroxy-containing poly(etherimide) (**PETI-OH**) and poly(esterimide) (**PESI-OH**) were described in our pervious papers.[32,36]

Synthesis of Chromophore-Functionalized Polymers. Polymers **PESI-X** and **PETI-X** were prepared by the substitution reaction of **PESI-OH** and **PETI-OH** with chromophores **AZ-1**−**AZ-7** via the Mitsunobu reaction.[32,36,37] Amounts of 1 mmol (0.67 g) of polyhydroxyimide, 1.1 mmol of the chromophore (**AZ-1**−**AZ-7**) and 1.6 mmol (0.42 g) of triphenylphosphine were dissolved in 7 mL of NMP. Then, the resulting solution was heated to 75−80 °C, and 1.6 mmol (0.28 g) of DEAD was added dropwise. The reaction mixture was further stirred at 75−80 °C for 24 h under the nitrogen atmosphere. The polymer was precipitated in the mixture of methanol (150 mL) and water (50 mL), filtered, and purified by the Soxhlet extraction with methanol for 72 h and dried at 105 °C in vacuum. Polymers **PESI-7** and **PETI-7** were reported in our pervious paper.[32,36]

PESI-1. ^{1}H NMR (DMSO-d_6, δ, ppm): 1.10 (t, CH_3, 3H), 1.69 (s, CH_3, 12H), 3.57 (t, CH_2, 2H), 3.79 (t, CH_2, 2H), 4.33 (q, CH_2, 2H), 6.69 (d, 2H), 7.00 (d, 2H), 7.09 (d, 8H), 7.29 (d, 4H), 7.32 (d, 4H), 7.48 (d, 8H), 7.52 (d, 4H), 7.62 (d, 2H), 7.82 (d, 2H), 7.95 (d, H), 8.18 (d, H), 8.29 (d, 2H), 8.45 (d, 2H), 8.58 (d, 2H), 10.39 (d, OH, H). FTIR (KBr, cm^{-1}): 3381 (OH), 2970, 2860 (CH_3, CH_2), 1783, 1728 (C═O in imide), 1367 (C−N stretching), 726 (C−N deformation), 1513, 1338 (NO_2), 1282, 1244 (−C−O−C−).

PESI-2. ^{1}H NMR (DMSO-d_6, δ, ppm): 1.18 (t, CH_3, 3H), 1.73 (s, CH_3, 12H), 3.6 (t, CH_2, 2H), 3.88 (t, CH_2, 2H), 4.59 (q, CH_2, 2H), 6.69 (d, 2H), 6.80 (d, 2H), 7.02 (d, 8H), 7.17 (d, 4H) 7.32 (d, 4H), 7.36 (d, 8H), 7.45 (d, 4H), 7.63 (d, 2H), 7.83 (d, 2H), 8.17 (d, H), 8.30 (d, H), 8.49 (d, 2H), 8.58 (d, 2H), 10.30 (d, OH, H). FTIR (KBr, cm^{-1}): 3353 (OH), 2968, 2855 (CH_3, CH_2), 2226 (CN), 1783, 1725 (C═O in imide), 1372 (C−N stretching), 726 (C−N deformation), 1287, 1246 (−C−O−C−).

PESI-3. ^{1}H NMR (DMSO-d_6, δ, ppm): 1.13 (t, CH_3, 3H), 1.71 (s, CH_3, 12H), 3.62 (t, CH_2, 2H), 3.88 (t, CH_2, 2H), 4.36 (q, CH_2, 2H), 6.67 (d, 2H), 6.75 (d, 2H), 7.03 (d, 8H), 7.31 (d, 4H), 7.35 (d, 4H), 7.46 (d, 8H), 7.52 (d, 4H), 7.64 (d, 2H), 7.83 (d, 2H), 8.16 (d, H), 8.30 (d, H), 8.47 (d, H), 8.57 (d, H),8.78 (s, H) 10.39 (d, OH, H). FTIR (KBr, cm^{-1}): 3373 (OH), 2969, 2865 (CH_3, CH_2), 1783, 1727 (C═O in imide), 1368 (C−N stretching), 726 (C−N deformation), 1511, 1339 (NO_2), 1285, 1246 (−C−O−C−).

PESI-4. ^{1}H NMR (DMSO-d_6, δ, ppm): 1.19 (t, CH_3, 3H), 1.71 (s, CH_3, 12H), 3.64 (t, CH_2, 2H), 3.88 (t, CH_2, 2H), 4.6 (q, CH_2, 2H), 6.67 (d, 2H), 6.80 (d, 2H), 7.03 (d, 8H), 7.15 (d, 4H) 7.31 (d, 4H), 7.35 (d, 8H), 7.46 (d, 4H), 7.63 (d, 2H), 7.85 (d, 2H), 8.16 (d, H), 8.31 (d, H), 8.47 (d, H), 8.50−8.65 (m, 2H), 10.39 (d, OH, H). FTIR (KBr, cm^{-1}): 3353 (OH), 2968, 2855 (CH_3, CH_2), 2226 (CN), 1783, 1726 (C═O in imide), 1370 (C−N stretching), 726 (C−N deformation), 1509, 1341 (NO_2), 1287, 1247 (−C−O−C−).

PESI-5. ^{1}H NMR (DMSO-d_6, δ, ppm): 1.15 (t, CH_3, 3H), 1.71 (s, CH_3, 12H), 3.52 (t, CH_2, 2H), 3.93 (t, CH_2, 2H), 4.10 (q, CH_2, 2H), 6.67 (d, 2H), 6.86 (d, 2H), 7.02 (d, 8H), 7.15 (d, 4H), 7.29 (d,, 4H), 7.31 (d, 8H), 7.35 (d, 4H), 7.46 (d, 2H), 7.79−7.84 (m, 4H), 7.96 (d, 2H), 8.16 (dd, H), 8.30 (dd, H), 8.48 (d, 2H), 8.58 (d, 2H), 10.41 (d, OH, H). FTIR (KBr, cm^{-1}): 3355 (OH), 2968, 2871 (CH_2), 1782, 1725 (C═O in imide),1373 (C−N stretching), 726 (C−N deformation), 1510, 1344 (NO_2), 1287, 1246 (−C−O−C−).

PESI-6. ^{1}H NMR (DMSO-d_6, δ, ppm): 1.25−1.40 (m, CH_2, 4H), 1.50−1.68 (m, CH_2, 4H), 1.72 (s, CH_3, 12H), 3.83−4.09 (m, CH_2, 4H), 7.05 (d, 8H), 7.16 (d, 4H), 7.28 (dd, 4H), 7.31 (d, 8H), 7.35 (d, 4H), 7.45 (d, 2H), 7.58 (d, 2H), 7.92 (d, 2H), 7.96 (d, 2H), 8.16 (dd, H), 8.35 (dd, H), 8.50 (d, 2H), 8.56 (d, 2H), 10.31 (d, OH, H). FTIR (KBr, cm^{-1}): 3360 (OH), 2968, 2870 (CH_3, CH_2), 1783, 1727 (C═O in imide), 1367 (C−N stretching), 725 (C−N deformation), 1508, 1343 (NO_2), 1285, 1247 (−C−O−C−).

PETI-1. ^{1}H NMR (DMSO-d_6, δ, ppm): 0.99 (t, CH_3, 3H), 1.68 (s, CH_3, 12H), 3.65−3.85 (m, CH_2, 4H), 4.29 (q, CH_2, 2H), 6.70 (d, 2H), 7.00 (d, 2H), 7.09 (d, 8H), 7.25 (d, 4H), 7.34 (d, 4H), 7.46 (d, 8H), 7.77 (d, 4H), 7.80 (d, 2H), 7.85−7.97 (m, 4H), 8.20−8.35 (m, 4H), 10.20 (s, OH, H). FTIR (KBr, cm^{-1}): 3370 (OH), 2967, 2860 (CH_3, CH_2), 1778, 1722 (C═O in imide), 1362 (C−N stretching), 745 (C−N deformation), 1506, 1337 (NO_2), 1272, 1235 (−C−O−C−).

PETI-2. ^{1}H NMR (DMSO-d_6, δ, ppm): 0.94 (t, CH_3, 3H), 1.64 (s, CH_3, 12H), 3.60−3.80 (m, CH_2, 4H), 4.24 (t, CH_2, 2H), 6.67 (d, 2H), 6.97 (d, 2H), 7.08 (d, 8H), 7.20 (d, 4H) 7.32 (d, 4H), 7.38 (d, 8H), 7.50 (d, 4H), 7.60 (d, 2H), 7.82 (m, 4H), 7.86 (m, 4H), 10.30 (d, OH, H). FTIR (KBr, cm^{-1}): 3360 (OH), 2968, 2855 (CH_3, CH_2), 2224 (CN), 1778, 1724 (C═O in imide), 1361 (C−N stretching), 745 (C−N deformation) 1272, 1235 (−C−O−C−).

PETI-3. ^{1}H NMR (DMSO-d_6, δ, ppm): 0.97 (t, CH_3, 3H), 1.67 (s, CH_3, 12H), 3.60−3.8 (m, CH_2, 4H), 4.27 (q, CH_2, 2H), 6.71 (d, 2H), 6.95 (d, 2H), 7.09 (d, 8H), 7.20−7.40 (m, 8H), 7.45 (d, 8H), 7.73 (d, 4H), 7.90 (d, 2H), 8.16 (d, 2H), 8.20−8.4 (m, 2H), 8.70−8.85 (m, 3H), 10.27 (d, OH, H). FTIR (KBr, cm^{-1}): 3370 (OH), 2968, 2860 (CH_3, CH_2), 1778, 1724 (C═O

TABLE 3: SEC Characterization and Reduced Viscosity (η_{red}) of Studied Azopolymers

		SEC (THF, PS)					
		conventional calibration detector: differential refractive index			universal calibration detector: differential refractive index with viscometer		
polymer code	η_{red}[a] [dL/g]	$M_w(\times 10^{-3})$	$M_n(\times 10^{-3})$	PD	$M_w(\times 10^{-3})$	$M_n(\times 10^{-3})$	PD
PESI-1	0.37						
PESI-2	0.18						
PESI-3	0.22	9.3	5.0	1.9	5.7	2.9	2.0
PESI-4	0.54	8.9	4.4	2.0	4.8	2.5	1.9
PESI-5	0.16	9.6	3.9	2.5	4.8	2.8	1.7
PESI-6	0.51	12.1	5.8	2.1	4.9	2.8	1.8
PESI-7	0.60						
PETI-1	0.41	28.0	8.0	3.5			
PETI-2	0.33	26.3	4.3	6.1			
PETI-3	0.30	30.5	7.2	4.2			
PETI-4	0.36	21.2	5.7	3.7			
PETI-6	0.62	25.6	9.5	2.7	20.8	7.3	2.8
PETI-7	0.66	22.6	6.6	3.4	16.7	4.2	4.0

[a] Reduced viscosity of the polymer measurement in NMP; concentration = 0.2 g/100 mL at a temperature of 25 °C.

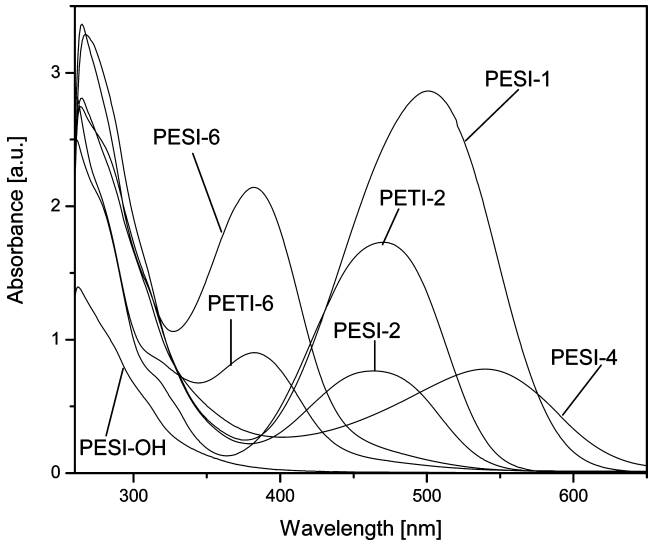

Figure 5. UV−vis spectra of the azobenzene-functionalized poly(esterimide)s and poly(etherimide)s.

TABLE 4: Absorption Maxima (λ_{max}) of the Polymers in NMP Solution and in Films Deposited onto Glass Slides and λ_{max} of the Chromophores in NMP Solution

	λ_{max}[nm]		
polymer code	in NMP	in film	in chromophore
PESI-OH	262, 287[a], 312[a]		
PESI-1	262, 283[a], 312[a], 501	486	500 (**AZ-1**)
PESI-2	267, 311[a], 463	458	479 (**AZ-2**)
PESI-3	266, 282[a], 309[a], 534	528	532 (**AZ-3**)
PESI-4	265, 284[a], 308[a], 540	538	548 (**AZ-4**)
PESI-5	267, 286[a], 310[a], 515	506	532 (**AZ-5**)
PESI-6	265, 282[a], 310[a], 382	380	383 (**AZ-6**)
PESI-7	265, 291[a], 312[a], 368	365, 470[a]	371 (**AZ-7**)
PETI-OH	262, 283[a], 320[a]		
PETI-1	275[a], 313[a], 500	304, 500	500 (**AZ-1**)
PETI-2	262, 282[a], 318[a], 471	459	479 (**AZ-2**)
PETI-3	263, 284[a], 320[a], 528	518	532 (**AZ-3**)
PETI-4	263, 284[a], 319[a], 544	546	548 (**AZ-4**)
PETI-6	262, 275[a], 313[a], 383	381	383 (**AZ-6**)
PETI-7	263, 367	366	371 (**AZ-7**)

[a] The position of absorption band calculated using the second derivatives method (i.e., the minimum of the second derivative of absorption corresponds to the absorption maximum).

in imide), 1362 (C−N stretching), 745 (C−N deformation), 1509, 1338 (NO_2), 1271, 1236 (−C−O−C−).

PETI-4. ^{1}H NMR (DMSO-d_6, δ, ppm): 1.00 (t, CH_3, 3H), 1.68 (s, CH_3, 12H), 3.70 (t, CH_2, 2H), 4.10 (t, CH_2, 2H), 4.30 (q, CH_2, 2H), 6.70−6.80 (m, 4H), 7.00 (d, 8H), 7.05−7.20 (m, 8H), 7.34 (d, 8H), 7.51 (d, 4H), 7.60 (d, 2H), 7.92 (d, 2H), 8.40−8.50 (m, 2H), 8.70−8.80 (m, 3H), 10.26 (s, OH, H). FTIR (KBr, cm^{-1}): 3360 (OH), 2968, 2855 (CH_3, CH_2), 2224 (CN), 1778, 1723 (C═O in imide), 1363 (C−N stretching), 746 (C−N deformation), 1505, 1338 (NO_2), 1273, 1236 (−C−O−C−).

PETI-6. ^{1}H NMR (DMSO-d_6, δ, ppm): 1.20−1.30 (m, CH_2, 4H), 1.69 (s, CH_3, 12H), 3.65−3.8 (m, CH_2, 4H), 3.90−4.10 (m, CH_2, 4H), 7.05 (d, 8H), 7.09−7.20 (m, 4H), 7.30 (d, 4H), 7.34 (d, 8H), 7.45 (d, 4H), 7.80−8.00 (m, 4H), 8.25−8.4 (m, 8H), 10.20 (s, OH, H). FTIR (KBr, cm^{-1}): 3350 (OH), 2964, 2862 (CH_3, CH_2), 1778, 1723 (C═O in imide), 1363 (C−N stretching), 746 (C−N deformation), 1504, 1343 (NO_2), 1272, 1235 (−C−O−C−).

Preparation of Polymer Film. The homogeneous solutions of azopolymers in NMP were filtered through 0.2 μm membranes and casted onto glass substrates. The residual solvent was removed from films by heating them for 2 h at 160−190 °C, near to the polymer T_g, that is, the temperature at which the polymer segmental motion is large enough to free possibly trapped solvent molecules. The film thickness was determined with an interference microscope (Tolansky method), and it was in the range of 0.36−2.92 μm.

Measurements. FTIR spectra were recorded on a BIO-RAD FTS 40 A spectrometer using KBr pellets. ^{1}H NMR spectroscopy was carried out on a Varian 300 spectrometer using DMSO-d_6 as a solvent and TMS as the internal standard. UV−vis spectra were recorded in a NMP solution of polymers and as films casted on glass substrates using a Jasco V570 UV−V−NIR spectrometer. The X-ray diffraction patterns on solid samples were recorded using Cu Kα radiation on a wide-angle HZG-4 diffractometer working in the typical Bragg geometry. Differential scanning calorimetry (DSC) measurements were done using a DuPont 1090B apparatus with a heating rate of 20 °C/min under the nitrogen atmosphere. Thermogravimetric analyses (TGA) were performed on a Paulik−Erdey apparatus at a heating rate of 10 °C/min under nitrogen. The reduced viscosity was measured in NMP (concentration = 0.2 g/100 mL) at 25 °C using a Ubbelohde viscometer. The

TABLE 5: The Polymer Glass Transition Temperatures (T_g) and Thermogravimetric Analyses (TGA)

polymer code	T_g[°C]	TGA T_d[a][°C]	T_{10}[b][°C]	T_{20}[c][°C]	char yield[d][%]
PESI-OH	225	406	433	486	41
PESI-1a	225				
PESI-1	175	307	315	334	43
PESI-2	201	313	353	404	34
PESI-3	199	296	329	417	44
PESI-4	209	322	362	452	45
PESI-5	214	281	317	374	44
PESI-6	168	352	367	399	38
PESI-7	167	368	382	424	39
PETI-OH	246	485	529	551	51
PETI-1a		230	270	530	50
PETI-1	213	275	325	520	55
PETI-2	195	320	330	460	50
PETI-3	199	290	513	505	50
PETI-4	228	360	470	540	50
PETI-6	196	370	423	480	50
PETI-7	181	446	476	525	57

[a] Decomposition temperature, determined by TGA in nitrogen, based on 5% weight loss. [b] Temperature of 10% weight loss. [c] Temperature of 20% weight loss. [d] Residual weight at 800 °C in nitrogen.

uniformity of the chromophore distribution in different molar mass fractions was determined by applying UV detection (variable wavelength UV detector, Spectra−Physics) after SEC analysis performed using a set of two PLgel 5 μm MIXED-C ultrahigh efficiency columns. Each of the investigated polymer samples was run twice with (i) detection at 255 nm characteristic for the polymeric backbone only and (ii) detection at 380 nm, at which the polymeric backbone was transparent and only the concentration of substituents was determined. Number average (M_n) and weight average (M_w) molecular weights and molecular weight distributions (M_w/M_n) of polymers were determined by SEC measurements conducted in THF at 35 °C with a flow rate of 1 mL/min using a set of two PLgel 5 μm MIXED-C ultrahigh efficiency columns. An isocratic pump (Spectra−Physics 8800) as a solvent delivery system, a differential refractive index detector (VE3580, Viscotek), and a viscometer detector (270 Dual Detector Array, viscometer only, Viscotek) were applied. A volume of 100 μL of the sample solution in THF (concentration of 2% w/v) was injected. Polystyrene standards with narrow molecular weight distributions were used to generate a universal calibration curve. The measurements of the light-induced optical anisotropy were performed using a holographic recording setup employing an Ar^+ laser working at line $\lambda = 514.5$ nm.[45] The same experimental conditions were applied for all polymers. The recording beams intensities were set equal to $I_{1,inc} = I_{2,inc} = 560$ mW/cm^2. The angle between writing beams was fixed at $\theta \cong 7.35°$, resulting in a periodicity of $\Lambda \cong 4.0$ μm (according to $\Lambda = \lambda/2 \sin(\theta/2)$). Diffraction gratings were recorded for s−s and s−p polarization configurations, and the exposure time lasted 30 min. After grating recording, the topography of the polymer surface at the illuminated area was examined by atomic force microscopy (Dimension V scanning probe microscope, Veeco) working in a tapping mode. The light-induced birefringence was measured in a Kerr-type experiment using excitation light from a YAG laser at 532 nm and a He−Ne laser light (632.8 nm) as a probe.

Results and Discussion

In this work, two types of azopolymers containing imide rings, that is, poly(esterimide)s (**PESI-X**) and poly(etherimide)s (**PETI-X**), were synthesized and characterized. Polymers differ in the structure of side-chain azobenzene chromophores and polymer backbone structures. Polymer properties were investigated from three points of view, (i) the effect of the kind of substituents on azobenzene groups, (ii) the structure of the spacer between the chromophore and the polymer backbone, and (iii) the presence in the polymer main-chain ester or ether linkages.

Initial attempts to prepare NLO polymers began with the synthesis of azobenzene chromophores. Chemical structures and synthetic approach for chromophores (**AZ-X**) are illustrated in Figure 1.

The chromophore abbreviated as **AZ-1** is known as Disperse Red 1, and it is commercially available. The chromophores **AZ-2**−**AZ-6** are new compounds, while the chromophore **AZ-7** has already been described in our previous work.[31] The azocompounds **AZ-2**−**AZ-5** were prepared by the azo coupling of 4-cyanoaniline, 2,4-nitroaniline, 2-cyan-4-nitroaniline, and Disperse Orange 3 with 2-(*N*-ethylanilino)ethanol. Synthesis of the chromophores **AZ-6** and **AZ-7** consisted of a few steps. First, the amino compounds were transferred to diazonium salts, the resulting salts were subjected to the conjugation reaction with phenol, and then, the aliphatic spacer was introduced into the chromophore by etherification with 6-chloro-1-hexanol to give dyes **AZ-6** and **AZ-7**. The UV−vis absorption spectra of

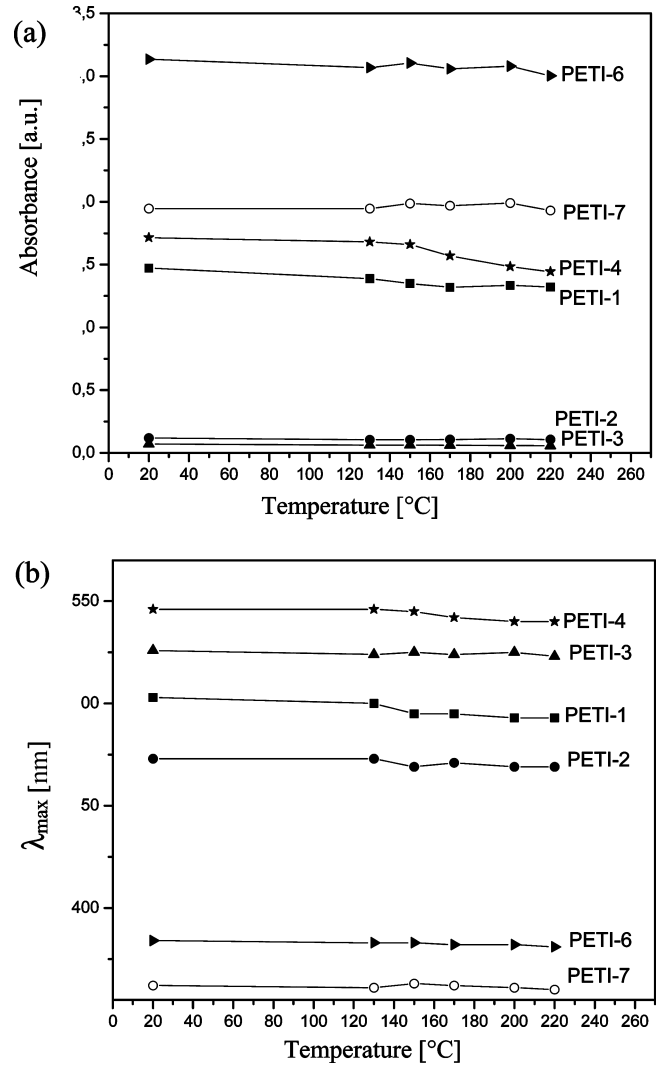

Figure 6. Relationship between temperature and (a) the relative intensity of absorbance and (b) the λ_{max} position in UV−vis spectra of poly(etherimide)s films.

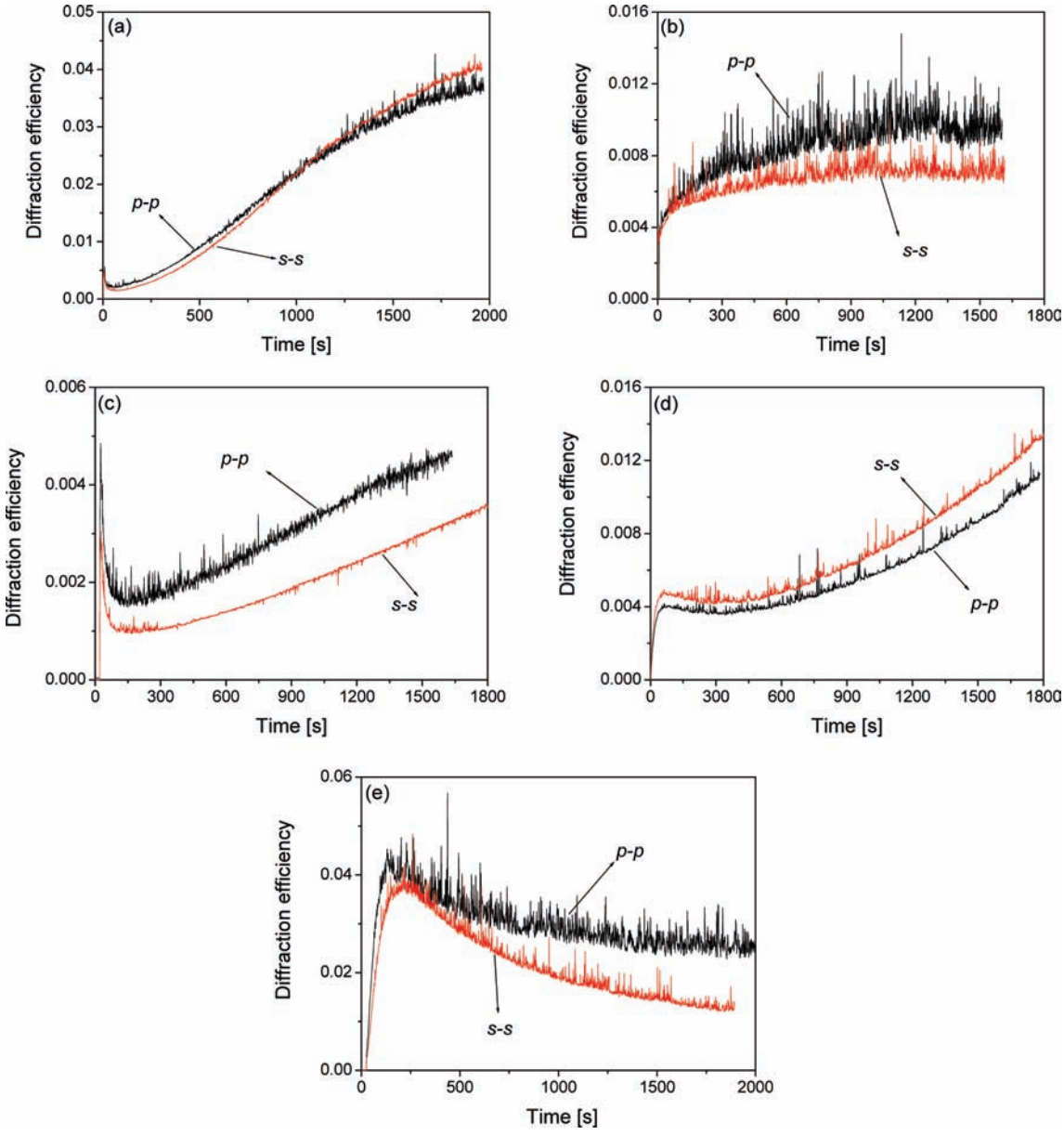

Figure 7. Diffraction efficiencies dynamics for polymers (a) **PESI-1**, (b) **PESI-2**, (c) **PETI-1**, (d) **PETI-3**, and (e) **PESI-7**.

azochromophores showed absorption peaks (λ_{max}) at the broad range from 371 to 548 nm, depending on their chemical structures. For chromophores **AZ-6** and **AZ-7** with alkoxy groups, the maximum was significantly hypsochromically shifted in comparison to other push−pull DR1-type chromophores, that is, containing additionally the tertiary amine group. In these chromophores, the electron-donating effect of the amino group in the π-conjugated donor−acceptor system shifted the position of λ_{max} bathochromically. In each series of azobenzene compounds, the position of λ_{max} depends upon the electron-withdrawing power of the acceptor group. Table 1 presents, calculated with the help of a MOPAC 2007 software, dipole moments of chromophores studied in this work along with their UV−vis absorption maxima.

The electron-withdrawing power of the azobenzene substituents decreases in the order NO_2/CN, NO_2/NO_2, NO_2, and CN, which is in a good accordance with the observed position of the absorption band maximum. The presence of double azo bond in the chromophore (**AZ-5**) shifted the position of λ_{max} to larger wavelengths in relation to the **AZ-1** dye containing one −N═N− linkage. According to Rau,[3] chromophores can be classified as "pseudo-stilbene" type molecules, which means that the high-energy $\pi-\pi^*$ transition is overlapping the low energy $n-\pi^*$ transition that leads to one intense absorption band for the trans isomer.

Polymer Synthesis and Characterization. The precursors without azobenzene groups, that is, polyhydroxy(esterimide) (**PESI-OH**) and polyhydroxy(etherimide) (**PETI-OH**) were obtained by polycondesation of 4,4′[diphenylopropane-di(benzene-4-estro-1,2-dicarboxylic)]anhydride and 4,4′-(4,4′-isopropylidenediphenoxy)bis(phthalic anhydride), respectively, with 2,4-diaminophenol dihydrochloride. The precursor of the azopolymer was transformed into respective chromophore-functionalized polyimides via a Mitsunobu reaction between the hydroxyl group of the chromophore and the phenol group on the polyimide backbone. The structures of the obtained NLO polymers are shown in Figure 2.

Instrumental techniques including FTIR and ^{1}H NMR spectroscopies were performed for the characterization of polymer molecular structures. The ^{1}H NMR spectrum of polyhydroxyimides showed the imidized structure with the phenolic hydroxyl proton peak at 10.40 ppm. As the Mitsunobu condensation

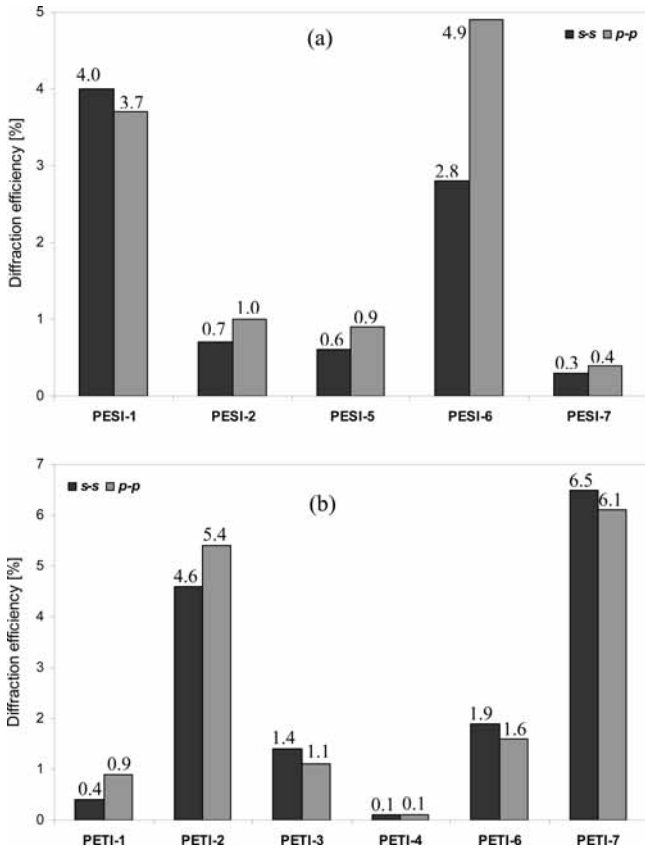

Figure 8. Maximum diffraction efficiencies measured for (a) poly(esterimide)s and (b) for poly(etherimide)s.

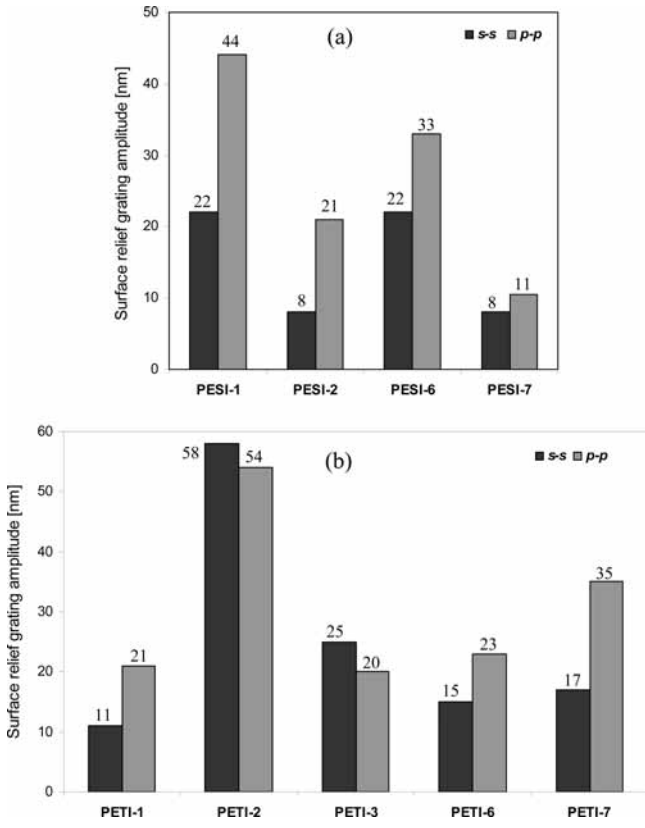

Figure 9. Surface relief grating modulation depths obtained in (a) poly(esterimide)s and (b) poly(etherimide)s films.

proceeds for loading of the chromophore into the polymer backbone, the phenolic proton peak decreased and new azobenzene peaks appeared in the range of 3.52−4.60 ppm due to aliphatic $-CH_2$ groups together with aromatic imide peaks. In FTIR spectra, all polymers exhibited characteristic imide absorption bands at around 1779 and 1726 cm^{-1} attributed to the asymmetric and symmetric stretching vibration of the carbonyl group in the five-membered imide ring. The absorption band at about 1362 cm^{-1} corresponds to the C−N stretching and that at 744 cm^{-1} to the imide ring deformation vibration, while the absorbance at around 2967 cm^{-1} is characteristic for vibration of methyl groups. The spectra of polyhydroxyimides showed the strong and broad absorption at around 3400 cm^{-1} characteristic for phenolic hydroxy groups. After the Mitsunobu condensation for the covalent bonding of chromophores onto the polymer backbone, new bands appeared in the FTIR spectra at ∼1338 and ∼1510 cm^{-1} due to the nitro group (**PESI-1**, **PETI-1**, **PESI-3**-**PESI-6**, and **PETI-3**-**PETI-6**) and at 2222 cm^{-1} due to the cyano group (**PESI-2**, **PETI-2**, **PESI-4**, **PETI-4**, **PESI-7**, and **PETI-7**). Meanwhile, the strength of the −OH absorption was significantly reduced. Additionally, the absorption band at about 2937 cm^{-1}, assigned to the vibration of $-CH_2$ groups coming from chromophores, was observed as well. Both ^1H NMR and FTIR spectral assignments supported the proposed structures.

In this study, the chromophore loading level of polymers was determined by UV−vis spectroscopy using the Beer−Lambert law.[38] The degree of the chromophore substitution in the polymer was calculated from the calibration curves obtained from UV−vis spectra of the chromophore solutions with various concentrations for each azo compound **AZ-X**. From the comparison of the peak absorbance of the polymer in solution with a known concentration and the calibration curve, the degree of functionalization was estimated. The calculated experimental percentage content of the chromophore in **PESI-OH** and **PETI-OH**, after the Mitsunobu reaction, is collected in Table 2.

With these methods, we find out that approximately 23−83% of hydroxy groups in hydroxypolymers **PESI-OH** and **PETI-OH** reacted with chromophores. The partial incorporation of the chromophores might be considered as an advantage since it provides more freedom for the molecular reorientation during trans ↔ cis isomerization cycles.[9]

The solubility of the synthesized polymers was determined for powdered samples using an excess of various solvents. All polymers could be easily soluble at room temperature in strong aprotic polar solvents such as NMP, DMSO, and DMA, protic solvent *m*-cresol, and in pyridine as well as in cyclohexanone (except for **PETI-5**). Poly(etherimide) with a chromophore which contained two azo bonds (**PETI-5**) was not soluble even in NMP, and because of that, it is was not investigated in the further part of this work due to the difficulty of thin-film preparation. Additionally, the solubility of the polymers was checked in such solvents as THF, chloroform, and acetonitrile. In this case, the polymer solubility was determined qualitatively by the dissolution of 2.5 mg of the solid polymer in 1 mL of organic solvent (at room temperature and at 50 °C), and the results are listed in Table 2. Comparing the influence of the chemical constitution of the polymer backbone on the solubility, it can be concluded that poly(esterimide)s (**PESI-X**) exhibited better solubility than poly(etherimide)s (**PETI-X**). After functionalization, polymers showed improved solubility with respect to corresponding precursor polymers. The increased solubility of polymers after functionalization may result from the increased size of the side chain, which leads to the decrease of the intermolecular interactions.

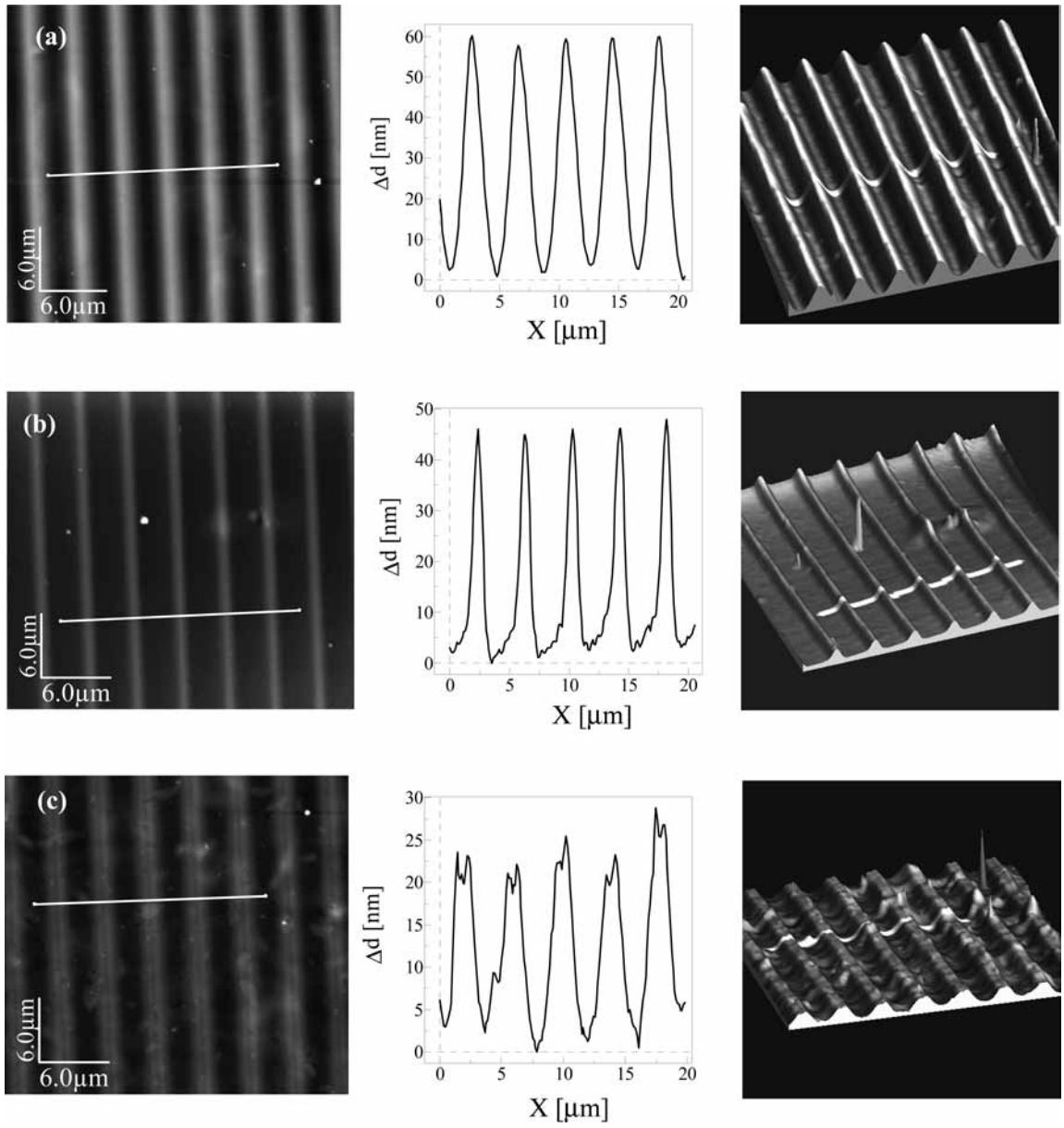

Figure 10. AFM polymer surface scans of (a) **PETI-2**, (b) **PESI-1**, and (c) **PETI-3**. Two- and three-dimensional topographies, to the left and to the right, respectively, and surface profiles in the middle.

The ideal material for many end-use optical applications should be highly amorphous as crystallites introduce unwanted light scattering. Thus, the supramolecular structure of the obtained polymer films was evaluated by wide-angle X-ray diffraction experiments. X-ray patterns for exemplary polymers are shown in Figure 3.

One broad diffraction peak of the diffusion type centered at 23° (2θ) was observed for all studied samples (cf. Figure 3). All polymers showed the same diffraction patterns typical for perfectly amorphous materials.

Since the postfunctionalization strategy is applied to develop NLO polymers and only partial chromophore loading level is achieved, the chromophore distribution in the polymer is not known. The topology of the chromophores in polymers, assuming that all polymer chains contained chromophores, was examined by a size-exclusion chromatography (SEC) with UV detectors working at wavelengths characteristic for the polymer backbone (255 nm) and the azobenzene trans isomer (380 nm). Only polymers with UV−vis absorption of the chromophore peaking at 380 nm were chosen for this investigation (**PESI-6**, **PETI-6**, and **PETI-7**). The obtained exemplary SEC elugrams for **PETI-7** are presented in Figure 4.

The elugram overlays illustrate the content of azobenzene groups in different molar mass fractions of the polymeric sample. It is clear that the synthesized polymers are characterized by a uniform chromophore functionalization along the entire molar mass distribution.

The molecular weight of the polymers was determined using SEC. In any case, the obtained values, similar to the values of viscosity, should be treated indicatively only since the calibration with polystyrene standards may result in questionable results when the polymers differ strongly from solvodynamic volumes of polystyrene.[39] To improve the conventional calibration, SEC results were recalculated according to universal calibration with use of an additional detector, that is, a viscometer. Due to a very uniform substitution of polymers, average values of refractive index increments were used for calculations. SEC analysis revealed a unimodal weight distribution, and results are colleted in Table 3.

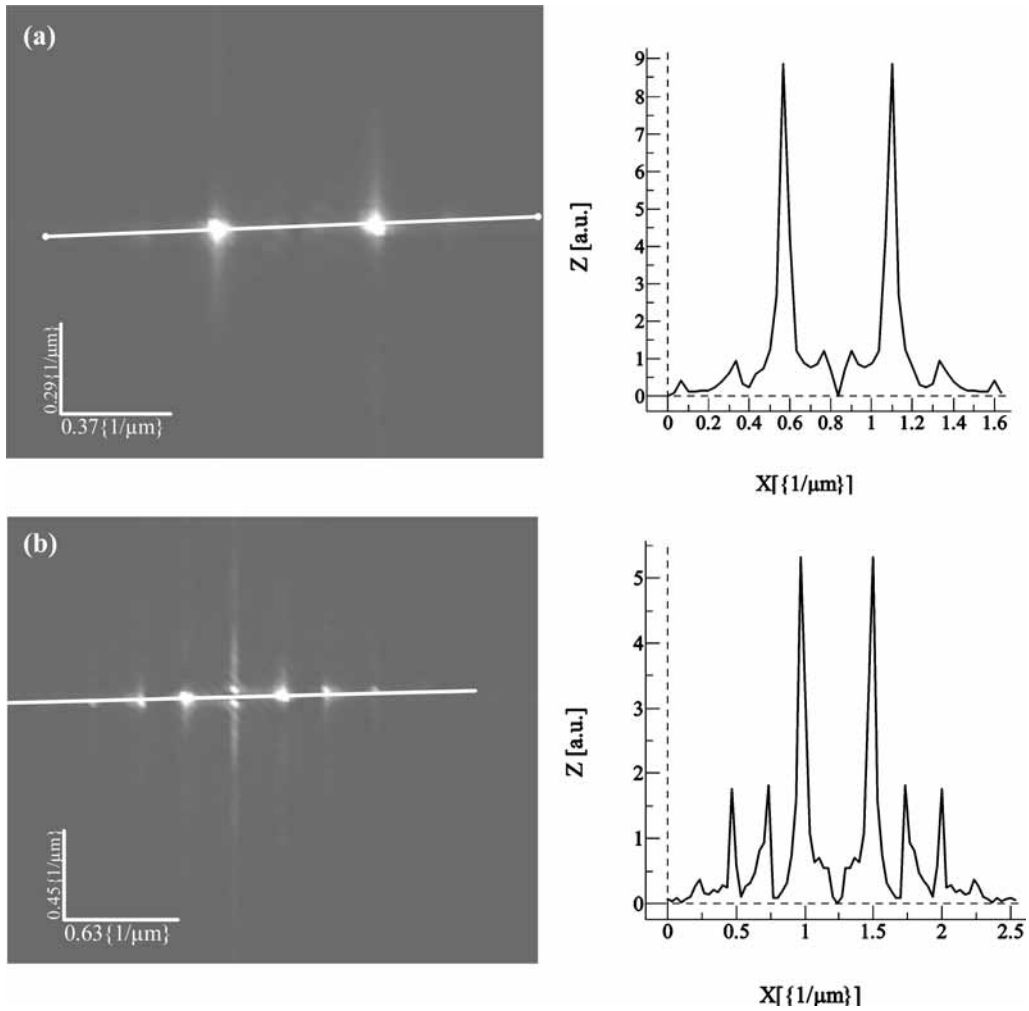

Figure 11. Fast Fourier transform spectra of SRGs for polymers (a) **PETI-2** and (b) **PESI-1** together with their profiles taken at the direction of the grating wave vector.

The synthesized polymers exhibited not high molecular weights. The molecular weight of the polymer can have considerable influence on the efficiency and the rate of the grating inscription process.[31] Polymers with moderate molecular weights are desirable for the holographic grating recording. It was found that the grating inscription and the surface relief grating formation in the high-molecular-weight azobenzene-functionalized polymers are less efficient than those in moderate weight ones, possibly due to expected chain entanglements.[15]

Linear Optical Properties. UV−vis spectra of poly(ester-imide)s and poly(etherimide)s were acquired both in NMP solution and in polymer films casted on a glass substrate. The range of UV−vis measurements was limited by the transparency of the used solvent and the substrate. The representative absorption spectra of **PESI-OH** and functionalized polymers are compared in Figure 5.

Absorption spectra of the studied azopolymers showed similar characteristics, that is, the strong band with the maximum located in the range of 382−544 nm and attributed to the electronic transition moment of the *trans*-azochromophore.[40] This band is clearly separated from the absorption in the UV in the range of 263−320 nm, characteristic of the transition within the polymer backbone. The precursors, that is, polyhydroxy-imides, exhibited no light absorption above 350 nm. The λ_{max} values of the azobenzene transition in chromophores and azo-functionalized polymers in NMP solution and in the form of films are collected in Table 4.

In most cases, positions of the azobenzene absorption band of polymers were slightly changed as compared to that of **AZ-X** compounds. A blue shift (about 4−17 nm) of the transition of the azobenzene between azopolymers and the chromophores **AZ-X** was observed, suggesting that polar properties of chromophores are not strongly affected by the incorporation of them into the polymer side chain. The highest hypsochromic shift was detected for polymers **PESI-2**, **PETI-2**, and **PESI-5** relative to its chromophores **AZ-2** and **AZ-5**. The blue shift may be attributed to the fact that the charge-transfer interaction between the electron acceptor ($-NO_2$ or $-CN$) and the resultant tertiary amine donor group was slightly reduced.[41] The λ_{max} positions were strongly affected by substituents on the azobenzene unit and the chemical constitution of the spacer bonding azobenzene unit with the polymer backbone. Polymers containing azobenzene with two substituents, that is, cyano and nitro (**PESI-4** and **PETI-4**), revealed the peak maximum of the azobenzene absorption band shifted bathochromically in comparison with the compounds containing other substituents. The presence of one nitro group in the azobenzene unit shifts hypsochromically the absorption maximum as compared to the cyano group. Significant differences were observed between positions of absorption bands of polymers containing chromophores tethered by alkoxy group ($-O-(CH_2)_6-O-$) and polymers possessing a spacer with a tertiary amine unit. The absorption maximum of polymers containing chromophores with the amine group (**AZ-1**- **AZ-5**) was red shifted (95−118 nm) in relation to the

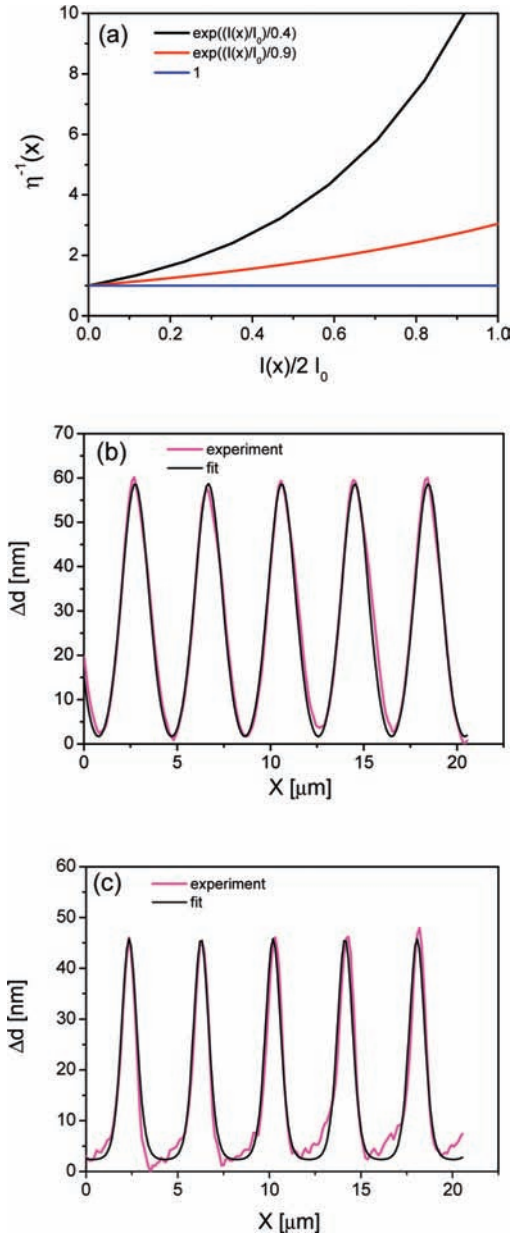

Figure 12. Profiles of surface relief gratings and their fit using the local polymer fluidity function $\eta^{-1}(x)$. (a) Plot of the $\eta^{-1}(x)$ function well approximated the observed reliefs for polymers (b) **PETI-2** and (c) **PESI-1**.

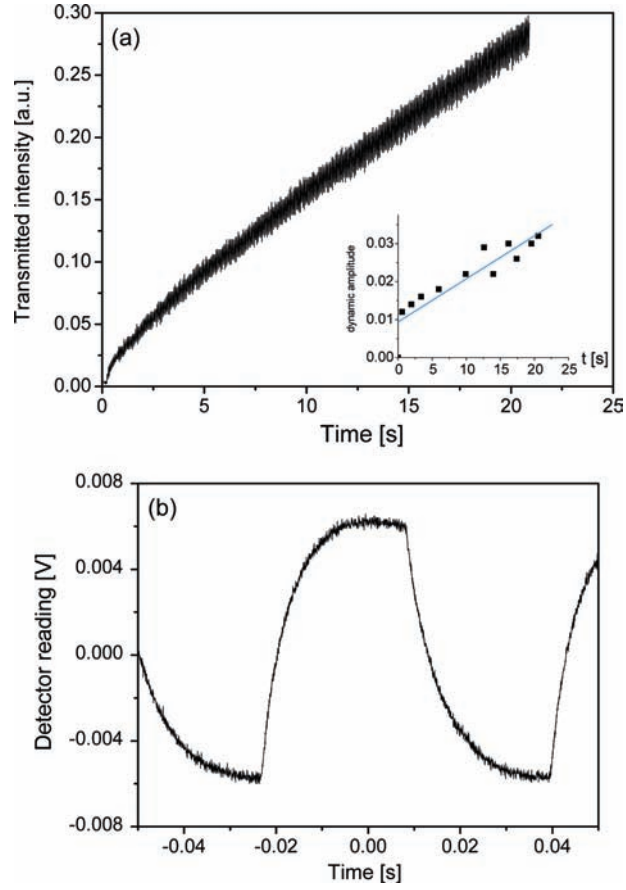

Figure 13. Example of measurements of 532 nm light-induced (a) static birefringence and (b) dynamic birefringence in **PESI-5** polymer film. Excitation light (532 nm) was chopped at a frequency of 15 Hz. The inset to (a) shows the temporal growth of the amplitude of the dynamic birefringence.

TABLE 6: Static and Dynamic (15 Hz) Parts of 532 nm Light-Induced Birefringence Measured at 632.8 nm in Polymeric Thin Films Using an Optical Kerr Gate

polymer code	d [μm]	dynamic Δn_d at 632.8 nm	static Δn_s at 632.8 nm	$\Delta n_d/\Delta n_s$
PESI-1	1.87	3.26×10^{-4}	5.60×10^{-3}	0.058
PESI-2	0.93	1.20×10^{-3}	5.94×10^{-3}	0.202
PESI-3	2.35	9.3×10^{-5}	2.67×10^{-4}	0.348
PESI-4	2.92	5.6×10^{-5}	2.55×10^{-4}	0.220
PESI-5	0.36	1.30×10^{-3}	6.33×10^{-3}	0.205
PESI-6	0.47	5.17×10^{-4}	1.20×10^{-2}	0.043

others with chromophores containing the alkoxy group (**AZ-6** and **AZ-7**) and the same substituent on the azobenzene unit. This large red shift can be explained by the difference in polarity of these two types of chromophores. Taking into account the dipole moment calculated for chromophores **AZ-X** (cf. Table 1), the stronger interaction between more polar chromophores in polymers (**PESI-1**−**PESI-5** and **PETI-1**−**PETI-4**) leads to improved planarity of the polymer chain and consequently to bathochromic shifts in the absorption maximum.

The absorption maximum in the polymer film was shifted to the shorter wavelength in comparison to that in the solution (by about 6−15 nm), indicating possible H-type aggregation of azobenzene chromophores in the film, similarly to what was observed for other azopolymers.[42−44]

Thermal Properties. The thermal behavior of polymers was evaluated by thermogravimetric analysis (TGA) in the nitrogen atmosphere and by a differential scanning calorimetry (DSC). The results are summarized in Table 5.

It is obvious that thermal properties depend on the structure of polymers, in this case, on the microstructure of the polymer backbone, the chromophore, and the extent of functionalization. Studied polymers exhibited no crystallization or melting temperature in DSC measurements. The glass transition temperature (T_g), defined by the midpoint of the baseline shift of polymers, ranged from 167 to 228 °C. Polyhydroxyimide-containing ether groups (**PETI-OH**) exhibited higher glass transition than the polymer with ester linkages (**PESI-OH**). This dependency was also seen in polymers with azobenzene moieties. It was observed that after the Mitsunobu reaction, the T_g of polymers decreased in comparison with the precursor polyhydroxyimide. DSC studies indicated that as the loading level of the NLO chromophore increased from 10 (**PESI-1a**) to 81% (**PESI-1**), the glass transition temperature of the polyimide decreased from 225 to 175 °C. Taking into account the chemical structure of the linkage group between the azobenzene moiety and the

polymer backbone, it was found that the T_g of polymers with the alkoxy spacer (**PETI-6** and **PETI-7**) was lower than that with the substituted amine group (**PETI-1** and **PETI-2**). We compared only polymers with the similar chromophore loading level. Obtained modified polyimides exhibited a higher T_g than polyimides reported by Chen et al.,[31] in which the glass transition temperature decreased up to 130 °C after the postfunctonalization. Azopolyimides prepared by the azo coupling reaction also showed the lower T_g.[29]

The decomposition temperature (T_d) (based on 5% weight loss) and the 10% weight loss temperatures (T_{10}), usually considered as the criterion in determining the thermal stability of high-temperature azopolymers, were in the ranges of 281−446 and 315−476 °C, respectively. Furthermore, the residual weights at 800 °C in nitrogen were in the range of 34−57%. The incorporation of azobenzene units into the polymer chain significantly lowered their thermal stability in comparison with patent polymers due to the ether linkages formed after the Mistunobu condensation. The lowering of T_d was connected with the decomposition of NLO chromophores. The effect of the kind of spacer between the polymer backbone and the azochromophore and the polymer backbone structure on the polymer thermal behavior was also detected. Similar as in T_g, a higher decomposition temperature exhibited poly(etherimide)s rather than poly(esterimide)s. The TGA trace of polymers **PETI-1a** and **PETI-1** supported the following argument: as the NLO chromophore loading levels increase, the weight loss increases accordingly. This substantial difference in the thermal stability of polymers with chromophores bonded with $-O-(CH_2)_6-O-$ and with the tether containing tertiary amine was observed. It was entirely due to the enhanced stabilities of alkoxy-substituted chromophores over their alkoxy-alkyloamino-substituted analogues.

Thermal properties of side-chain NLO poly(etherimide)s films were indicated with the help of UV−vis spectroscopy.[45] Each thin film of the polymer after deposition was heated to 130, 150, 170, 200, and 220 °C and kept at that temperature for 15 min. Each absorption spectrum was recorded, and the changes in the absorbance characteristic for the azobenzene group transition are shown in Figure 6.

Taking into account the temperature-induced changes in the absorbance (cf. Figure 6a), it was found that polymers retained from 100 to 84% of theirs original absorbance at 220 °C. In polymers with the spacer between the polymer chain and the azobenzene group with the tertiary amine **PETI-1**−**PETI-4**, the relative absorbance decreased by about 16−10%, while in polymers with the alkoxy group (**PETI-6** and **PETI-7**), the absorbance changed slightly (∼4%). Furthermore, poly(esterimide)s retained almost their original position of the absorption maximum of the azobenzene trans isomer at the investigated temperature range. The position of λ_{max} during heating was insignificantly shifted to shorter wavelengths by 2−10 nm. It should be pointed out that the obtained NLO polymers satisfy the demand of the high thermal stability required for the optical device fabrication.

Photoinduced Optical Anisotropy. Photoinduced optical anisotropy in azo-functionalized polymer films was studied by the holographic diffraction grating recording for all synthesized polymers and supplemented by measurements of the laser-light-induced birefringence for poly(esterimide)s **PESI-1**−**PESI-6.** The prepared azopolymers shown absorption band characteristics for transition of the trans isomer located in the large range of the visible spectrum. This feature is interesting because it provides the opportunity for creation of the photoinduced phenomena using various laser wavelengths. However, in this particular study, we used the single laser line for the investigation of the relation between the polymer architecture and photoinduced properties.

Holographic Diffraction Grating Recording. Irradiation of amorphous azo-functionalized polymer films by two interfering polarized laser beams induces a spatial optical anisotropy in the bulk of a material, that is, diffraction grating. However, the volumetric changes of optical properties are usually accompanied by the periodic surface corrugation of the free side of a film deposited on a glass substrate (formation of the surface relief grating). The dynamics and the strength of these light-induced effects can be measured simultaneously during the holographic grating recording process by the observation of the temporal evolution of the first-order diffraction efficiency ($\eta(t)$). The light diffraction efficiency is a function of an imposed material anisotropy (modulation of the refractive index and absorption coefficient) and a light wavelength and is defined as the ratio between the first-order diffracted light beam intensity ($I_{1,\mathrm{diff}}^{\pm 1}$) and the input beam intensity ($I_{1(2),\mathrm{inc}}$). The diffraction efficiency indirectly measures the light-induced difference of the refractive index of the material in the bright and dark part of fringes, the light-induced dichroism, as well as the magnitude of the surface relief depth. Contributions to the diffraction efficiency coming from different gratings can be separated, but this requires a complex analysis and additional precise measurements, for example, the surface topography by AFM.[46] However, the advantage of this technique is that it supports immediate information about the material ability to record information. The efficiency of the grating formation in photochromic polymer was found to depend on experimental conditions, such as light intensity, beam polarization, and intersection angle,[15,47−51] but it also depends on the chemical structures of the polymer backbone and the azobenzene group[52] or the polymer molecular weight.[53−55]

In the present studies, two polarization geometries were used for the grating inscription, s−s and p−p. The s−s polarization configuration means that both beams are linearly polarized with the E vector of the light perpendicular to the beam's incidence plane, whereas the p−p geometry denotes also linearly polarized beams with the E vector lying in the plane of the beam's incidence. Diffraction gratings were successfully recorded in almost all poly(esterimide)s and poly(etherimide)s for both polarization configurations, with the exception of **PESI-3** and **PESI-4** polymers. Exemplary results of the diffraction efficiency dynamics measured during the grating recording process in chosen poly(esterimide)s and poly(etherimide)s for both polarization geometries are shown in Figure 7.

It is known that during the grating recording process in azo-functionalized polymers, three diffraction gratings are formed.[56] One of them originates from the refractive index changes in the bulk of the material, the second from the thickness modulation (the surface relief grating), and the third one from the absorption coefficient changes. Therefore, the measured diffraction efficiency dynamics is the result of the light diffraction on all of these gratings, formed with different amplitudes and different recording time constants, and sometimes depends on their mutual phase shifts. Many different, that is, exponential and nonexponential, behaviors of the diffraction efficiency were measured; discussed here are the azopolymers (cf. Figure 7). The most interesting $\eta(t)$ dependences seem to be these complex ones (Figure 7a,c−e), where the diffraction efficiency increased rapidly at the beginning of the recording process, started to decrease, reaching the minimum, and

increased again. The decrease of the $\eta(t)$ is the result of the formation of two gratings shifted in phase.[56] The minimum of diffraction is observed when the amplitudes of these two gratings are comparable. After some time of the recording, when the first grating had already reached its maximum amplitude, the second grating was still formed, and its amplitude was increasing; thus the diffraction efficiency increased again. One can find the detailed explanation of the different diffraction efficiency dynamics in azopolymers in ref 56.

The results of comparison of the diffraction efficiency dynamics for s−s and p−p were surprising because there was no difference in $\eta(t)$ between these configurations (cf. Figure 7). One could expect the difference in the diffraction efficiency dynamics since the s−s configuration is significantly less effective in the surface relief grating formation process than the p−p one.[48,50,57] It is hard to find an explanation of such unexpected behavior of $\eta(t)$ for s−s and p−p in the group of studied azobenzene-functionalized polymers, which is completely different from that reported in the literature so far.[48,50] Experiments of the grating formation for each configuration were performed twice, diffraction efficiency dynamics were reproducible, and every time, the behaviors of $\eta(t)$ were very similar for both geometries.

The maximum diffraction efficiencies (η_{max}) measured in poly(esterimide)s and poly(etherimide)s under the same experimental conditions for both polarization geometries are gathered in Figure 8a for **PESIs** and in Figure 8b for **PETIs**.

We would like to stress that the discussion about the diffraction efficiency can be performed only when we assume that the thicknesses of polymer films are comparable. In the case of the studied polymers, the thicknesses were, more or less, comparable. The diffraction efficiencies for both polarization configurations were comparable. The inscribed diffraction gratings showed diffraction efficiencies in the range of 0.1−6.5% (cf. Figure 8).

After the inscription of holographic diffraction gratings, the polymer films were tested by the atomic force microscopy technique in order to estimate the surface grating modulation depth. The AFM topography scans were taken for a 20 μm × 20 μm area. The surface relief gratings were formed in all studied polymers, with the exception of polymers **PESI-5** and **PETI-4**. The results of AFM measurements are compared in Figure 9a for poly(esterimide)s and in Figure 9b for poly(etherimide)s. The modulation depths were in the range from 15 to 58 nm.

The diffraction grating inscription, that is, the dynamics and the diffraction efficiency, as well as the surface grating modulation depth was discussed from three points of view, (i) the effect of kind of substituents on azobenzene groups, (ii) the structure of the spacer between the chromophore and the polymer backbone, and (iii) the structure of the polymer main chain. The influence of the chemical structure of the polymer chain, that is, the presence in the polyimide of the ester or the ether linkages, on the grating formation process can be analyzed in polymers with the same two chromophore types and their content in the polymer. Taking into account these assumptions, to find the relationship between the polyimide backbone structure and the diffraction grating inscription efficiency, the following polymer pairs were compared: **PESI-3** with **PETI-3**, **PESI-4** with **PETI-4**, and **PESI-7** with **PETI-7**. Unexpected in polymers **PESI-3** and **PESI-4**, the holographic diffraction gratings were not formed at applied experimental conditions. Comparing the dynamics of $\eta(t)$ for poly(esterimide) **PESI-7** (not shown) and the poly(etherimide) analogue **PETI-7**, which is shown in Figure 7e, similar behavior was observed. The diffraction efficiency was six time higher for **PETI-7** than that for **PESI-7** (cf. Figure 8). Also, the relief grating in **PETI-7** showed a higher modulation depth (cf. Figure 9) than in its poly(esterimide) analogue. On the surface, the relief grating formation ability can influence, among other things, the glass transition temperature and the molecular weight of polymers. However, the compared polymers (**PESI-7** and **PETI-7**) exhibited a similar T_g and reduced viscosity. Moreover, these polymers absorbed UV−vis light in the same range. The obtained results suggest that the holographic grating recording process is more efficient in the polyimide in which the ether groups were introduced than in the polyimide in which the ester linkages were present. However, the contrary results were obtained in our previous work,[36] in which both the diffraction efficiency and the relief depth were slightly higher for poly(esterimide)s than for poly(etherimide)s. The conclusion in ref 36 was made by comparing a few poly(esterimide)s with a few poly(etherimide)s, whereas the conclusion in this paper was obtained on the basis of comparison of only the **PESI-7** with **PETI-7**, which suggests that one should rather believe in the results reported in ref 36. The most likely explanation of the discrepancy between these two reports is the difference in the polymer film thickness, which has significant influence on the photoinduced properties.[6]

It was found that the kind of the substituent on the chromophore moiety and the structure of the spacer between the polymer main chain and the azobenzene derivative influence the diffraction grating recording process. Comparing the diffraction efficiency dynamics in following polymers, **PESI-6** (not shown) with **PESI-7** (Figure 7e), **PETI-1** (Figure 7c) with **PETI-3** (Figure 7d), and **PETI-2** with **PETI-4** (both not shown), one can observe the influence of the substituent on the azobenzene group. The dynamics of the grating formation in the polymer containing the chromophore with the nitro group (**PESI-6**) exhibited exponential growth, whereas in the polymer with the cyano substituent (**PESI-7**), $\eta(t)$ increased and then started to slowly decrease to the minimum, which could have been observed for a little longer recording time. In polymers with two substituents in azobenzene groups **PETI-3** and **PETI-4**, a much lower decrease in the diffraction efficiency, after the increase at the beginning of the recording, was observed than that in polymers with one substituent **PETI-1** and **PETI-2** (cf. Figure 7d and c). Higher diffraction efficiency and deeper surface relief grating modulation were obtained in the polymer with the nitro group in the chromophore (**PESI-6**) than those in the polymer with the cyano substituent on the azobenzene moieties (**PESI-7**), despite, the higher chromophore content in **PESI-7**. These polymers characterized the same T_g and molecular weights, and the maximum of the absorption band of **PESI-6** was only slightly bathochromic shifted (15 nm) in comparison with **PESI-7**.

The introduction of the second substituent, that is, CN into the azobenzene group containing the nitro group at the para position to the azo bond (**PETI-4**), resulted in lowering of the diffraction efficiency in comparison with the polymer in which the chromophore possessed only NO_2 (**PETI-2**), despite, the higher chromophore content in **PESI-4**. In the case of **PETI-4**, the relief grating was not formed. These polymers differed in the UV−vis absorption range; the λ_{max} of **PETI-4** was about 46 nm bathochromically shifted in relation to **PETI-1**. On the other hand, introduction of the second NO_2 moiety (**PETI-3**) resulted in a higher diffraction efficiency and surface relief modulation depth in relation to the polymer with one nitro group (**PETI-1**).

The chemical structure of the spacer between azobenzene moieties and the polymer backbone also influenced the holographic grating recording process. This was concluded from taking into consideration the polymers pairs **PETI-2** with **PETI-7**, **PETI-1** with **PETI-6**, and **PESI-1** with **PESI-6**. By analyzing the dynamics of the grating formation in polymers that differ in the spacer structure, a clear conclusion cannot be drawn, that is, the diffraction grating efficiency dynamics exhibited exponential or nonexponential behavior during the recording process. It was found that in polymers with the spacer containing an alkoxy group (**PETI-7** and **PETI-6**) that the diffraction efficiency reached a higher value than in polymers with the tertiary amine group in the spacer (**PETI-2** and **PETI-1**) (Figure 8).

By comparing the surface modulation in these polymers, a clear conclusion cannot be drawn. From one side, the surface modulation was deeper in polymer **PETI-2** with the tertiary amine group in the spacer than that in polymer **PETI-7**, whereas for the other polymer pair **PETI-1** and **PETI-6**, the modulation depths were comparable (cf. Figure 9).

Additionally, the relation between the presence in chromophores of one or two azo bonds can be discussed in polymers **PESI-2** and **PESI-5**. In both polymers, exponential growth of the diffraction grating was observed. These polymers possess also different substituents in the chromophore; however, relevant to the earlier discussed results, deeper surface modulation was expected in the polymer with a nitro group (**PESI-5**) than in the polymer with CN (**PESI-2**). As it was mentioned previously, the surface relief grating was not detected in the polymer with two azo linkages (**PESI-5**), despite, a twice higher chromophore content in this polymer and the presence of a nitro moiety in comparison to the polymer with one azo bond in the azobenzene group (**PESI-2**). It can be concluded that the introduction of bis(azo) linkage units into the polymer seems to results in less efficient SRG fabrication.[58,59] In the case of polymers with bis(azobenzene) moieties, two azo bonds have to photoisomerize in the same structural unit; thus the alignment in the direction perpendicular to the light polarization is slower since it requires more cycles of trans ↔ cis isomerization It is easier to make the chain movements, caused by isomerized groups, in the polymer where the only one azo bond is present in the chromophore group.

Additionally, the SRG shapes in the investigated polymers should be mentioned. The film surfaces before the interference light exposure were planar without any regular periodicity. After completing the grating recording, the polymer film surface showed, in most cases, a near-sinusoidal shape. In the two polymers **PESI-1** and **PETI-3**, different surface modulation was observed. The surface relief gratings and their surface profiles are shown in Figure 10.

The shapes of the SRGs were either near-sinusoidal, which predominated (cf. Figure 10a), strongly deformed (cf. Figure 10b), or showed a tiny valley at the corrugation center (cf. Figure 10c). The surface modulations shown in Figure 10b and c were the same for both polarization configurations. The surface relief grating AFM topographies presented in Figure 10 for polymers **PETI-2** and **PESI-1** were analyzed with the 2-D fast Fourier transform (FFT) method. Results, in the form of power spectra of FFT, are shown in Figure 11, reflecting the differences in grating shapes.

Three strong peaks seen in the FFT spectrum for **PESI-1** (cf. Figure 11b) versus only one for **PETI-2** (Figure 11a) suggests that in the latter case, one deals with a near-sinusoidal shape, whereas in the former one, the grating is strongly deformed. Under the same conditions of illumination (we assume that the light intensity pattern was sinusoidal (e.g., $I(x) = I_0(1 + \cos(\mathbf{K}x))$, where $I_0 = 2I_{1,\mathrm{inc}}$), the difference in shape is due to a nonlinear process linked with the diffusion of polymer chains from illuminated to dark regions of the fringe pattern. Such a process is directly connected with the local temperature rise $T(x) \propto I(x)$ in the polymer film due to the light absorption by azochromophores. Since **PESI-1** absorbed more light at the laser working line, that is, 514.5 nm, than **PETI-2** (cf. Table 4), the strong polymer surface deformation is observed for the first polymer. Position (x)-dependent thermal agitation of the polymer chain mobility supported by mechanical forces (due to trans ↔ cis multiple photoisomerizations) leads to the polymer mass redistribution close to the free surface of the film. The chain mobility (polymer fluidity) is inversely proportional to the viscosity coefficient, which, according to the Vogel−Fulcher relation,[60] is given as $\eta(T) = B\exp(T_A/(T - T_V))$, where T_V is a Vogel temperature (typically 50 °C below T_g) and T_A is an "activation temperature" associated with the movement of molecules. In order to qualitatively describe the chain mobility process, we have assumed that under the low-light signal approximation, the local polymer fluidity $\eta^{-1}(x)$ is described by an exponential function of the form $\eta^{-1}(x) = \exp[(I(x)/2I_0)/m]$, where the m parameter describes the polymer chain flow nonlinearity (e.g., $m = 1$ describes a linear response, whereas $m < 1$ describes a nonlinear one). In Figure 12a, we present two $\eta^{-1}(x)$ functions, which, when applied to the sinusoidal interference pattern, reproduce well the measured SRG shapes (cf. Figure 12b and c).

Thus, the observed deviations from a perfectly sinusoidal interference pattern resulting from a local temperature rise were characteristic for polymers in which the position of λ_{max} was closer to the wavelength of laser light (cf. Figure 10c). The slight asymmetric distortion observed in the shape of the SRG seen in Figure 12c is related to the appearance of the phase shift between the interference pattern and the diffraction grating due to some breaking symmetry process in recording usually introduced into the system via asymmetric experimental conditions.

Photoinduced Birefringence. Any light-imposed molecular reorientation in azo-functionalized polymer films results in creation of in-plane optical anisotropy, birefringence and dichroism. In order to measure birefringence, one should choose the light of a wavelength that is not absorbed by a material. Optically induced birefringence was investigated by exposing polymer films to strongly absorbed linearly polarized laser light. We used a standard optical Kerr effect setup in which birefringence in the polymer film was induced by the green light delivered by a doubled-in-frequency cw YAG laser operating at 532 nm. The pumping beam polarized linearly at an azimuthal angle of 45° is incident normally on the sample and produces birefringence in the initially isotropic material via chromophore reorientations. A smaller in diameter linearly polarized probe beam at an angle of 0°and a wavelength of 632.8 nm reads the induced birefringence as the part of the light intensity passes through an analyzer set at an angle of 90°. Birefringence $\Delta n(I,\lambda)$ is here understood as a difference between refractive indices in the polymer within the plane of the sample parallel and perpendicular to the linear polarization direction of the 532 nm pumping light $\Delta n(I,\lambda) = n_{\|} - n_{\perp}$. Under equilibrium conditions, photoinduced birefringence $\Delta n(I,\lambda)$ at 632.8 nm is related to the accumulated by a probe light change of phase $\Delta\phi$ equal to

$$\Delta\phi(I,\lambda) = \frac{2\pi\Delta n(I,\lambda)d}{\lambda} \qquad (2)$$

where λ is the wavelength of the probing beam and d is the sample thickness. Birefringence is calculated from measurements of the probe laser light (632.8 nm) transmission through a sample (treated as a pure retardation plate for this wavelength) inserted between a system of crossed polarizers. A silicon detector system with a preamplifier was fed into four-chanel digital oscilloscope and calibrated. The experimental system allows for measurements of the dynamics of birefringence build-up at steady illumination conditions and, by chopping pumping light, at frequencies from 1 Hz to 1 kHz. Here, we report measurements of the photoinduced birefringence in polymers **PESI-2**−**PESI-6** under photostationary conditions (Δn_s saturated value of birefringence) as well as its dynamic part Δn_d, being reversible within the light chopping period (chopper frequency of $f = 15$ Hz). The former, that is, the saturated value of te birefringence Δn_s, is related to the amount of ordering superimposed by the light at given illumination conditions. The latter Δn_d informs about the reorientational effect related to those NLO chromophores which are not frozen in the polymeric matrix and could effectively react upon changing the conditions of illumination. It should be noted here that the dynamic birefringence was stable in time in the studied polymers even for the long lasting experiment, but its magnitude was dependent on the green light illumination level and the sample absorption at that particular wavelength. In this experiment, pure birefringence at 632.8 nm was measured, which reflects light induced ordering in a material. The ratio of dynamic part of the birefringence to the static one, for the same sample, carries information about the material's ability to permanently or temporarily record information. The results of the light-induced birefringence are gathered in Table 6.

The highest static optically induced birefringence among the studied polymers shows **PESI-6**. In-plane birefringence on the order of 0.01 is really large. The highest dynamic birefringence was observed in **PESI-5**, being on the order of 0.001. For permanent holographic grating recording, the most suitable is polymer **PESI-6**, having the smallest ratio $\Delta n_d/\Delta n_s$, while for dynamic holography, the most suitable is the polymer with the high ratio $\Delta n_d/\Delta n_s$ accompanied by a high value of dynamic birefringence, for example, **PESI-5** and **PESI-2**. These results nicely correspond to values of the polymer reduced viscosities shown in Table 3. **PESI-6** is highly viscous ($\eta^*_{red} = 0.51$ dL/g), thus promoting the permanent orientation of chromophores, while polymers **PESI-5** and **PESI-2** have the smallest reduced viscosities ($\eta^*_{red} = 0.16$ and 0.18 dL/g, respectively), which make the dynamics of the chromophore reorientation enhanced. In Figure 13, we show an example of measurements of light-induced static and dynamic birefringence in **PESI-5**.

It is interesting to note that there is a linear growth of amplitude of the dynamic part of the birefringence with respect to static one at least at the small signal approximation. The measurements of static and dynamic parts of birefringence are complementary to measurements of holographic grating recording as they supply information about the optical properties of the studied materials.

Conclusions

The new poly(esterimide)s and poly(etherimide)s with photoisomerizable azobenzene groups were synthesized and characterized. Chromophore-functionalized polymers exhibited a good thermal stability with high T_g and very good solubility in most cases. The polymer properties, including the photoinduced one, were investigated from a few points of view, the effect of the structure of both the polymer main chain and the linkage between azobenzene units and the polymer backbone as well as the kind of substituents on azobenzene groups. Taking into account the diffraction efficiency and the surface modulation amplitude, higher values were obtained in poly(etherimide)s. Introduction of two nitro groups as substituents on azobenzene moieties and the presence of one azo bond resulted in a higher diffraction efficiency and deeper polymer surface modulation than in other investigated polymers. The holographic grating recording process was more efficient in polymers in which azobenzene groups were incorporated by the alkoxy spacer than that in polymers with the linkage containing a tertiary amine group. In polymers with the alkoxy spacer and the nitro group, the highest static optically induced birefringence on the order of 0.01 was measured. On the other hand, polymers containing the tertiary amine group showed high ratios $\Delta n_d/\Delta n_s$, which is more suitable for the dynamic holography.

Due to the fact that efficient relief gratings can be easily recorded on these polymers film, they may found to have potential applications in optical devices and optical element fabrication. This study is expected to be useful for the development of the polyimide for photonics branch of science and to optimize the material design for diverse optical application using azobenzene polyimides.

Acknowledgment. This research was supported by the Polish Ministry of Education and Science, Grants N205 037 31/1700 (E.S.-B.) and N507 132 31/3302 (A.S. and A.M.). One of the authors (A.S.) is the laureate of The Domestic Grant for Young Scientists awarded by the Foundation for Polish Science. The authors thank to Dr. B. Jarzabek for UV−vis measurements.

References and Notes

(1) Yaroshchuk, O. V.; Dumont, M.; Zakrevskyy, Y. A.; Bidna, T. V.; Lindau, J. *J. Phys. Chem. B* **2004**, *108*, 4647.
(2) Yesodha, S. K.; Pillai, C. K. S.; Tsutsumi, N. *Prog. Polym. Sci.* **2004**, *29*, 45.
(3) Rau. H. In *Photochemistry and Photophysics*; Rabek, F. J., Ed.; CRC: Boca Raton, FL, 1990; Vol. II, Chapter 4, pp 119−141.
(4) Sekkat, Z.; Wodo, J.; Aust, E. F.; Knoll, W.; Volksen, W.; Miller, R. D. *J. Opt. Soc. Am. B* **1996**, *13*, 1713.
(5) Burland, D. M.; Miller, R. D.; Walsh, C. A. *Chem. Rev.* **1994**, *94*, 127.
(6) Cojocariu, C.; Rochon, P. *Pure Appl. Chem.* **2004**, *76*, 1479.
(7) Janik, R.; Kucharski, S.; Kubanska, A.; Lyko, B. *Pol. J. Chem.* **2001**, *75*, 241.
(8) Chang, Ch.-J.; Whang, W.-T.; Hsu, Ch.-Ch.; Ding, Z.-Y.; Hsu, K.-Y.; Lin, Sh.-H. *Macromolecules* **1999**, *32*, 5637.
(9) Ortyl, E.; Kucharski, S.; Gotszalk, T. *Thin Solid Films* **2005**, *479*, 288.
(10) Kim, D. Y.; Tripathy, S. K.; Li, L.; Kumar, J. *Appl. Phys. Lett.* **1995**, *66*, 1166.
(11) He, Y.; Wang, X.; Zhou, Q. *Polymer* **2002**, *43*, 7325.
(12) He, Y.; Yin, J.; Che, P.; Wang, X. *Eur. Polym J.* **2006**, *42*, 292.
(13) Fernandez, R.; Mondragon, I.; Oyanguren, P. A.; Galante, M. J. *React. Funct. Polym.* **2008**, *68*, 70.
(14) Xu, Z. S.; Drnoyan, V.; Natansohn, A.; Rochon, P. *J. Polym. Sci., Part A: Polym. Chem.* **2000**, *38*, 2245.
(15) Viswanathan, N. K.; Kim, D. Y.; Bian, Sh.; Williams, J.; Liu, W.; Li, L.; Samuelson, L.; Kumar, J.; Tripathy, S. K. *J. Mater. Chem* **1999**, *9*, 1941.
(16) Natansohn, A.; Rochon, P. *Chem. Rev.* **2002**, *102*, 4139.
(17) Ghosh, M. K., Mittal K. L., Eds. *Polyimides: Fundamentals and Applications*; Marcel Dekker Inc.: New York, 1996.
(18) Hasegawa, M.; Horie, K. *Prog. Polym. Sci.* **2001**, *26*, 259.
(19) Kim, T.-D.; Lee, K.-S.; Lee, G. U.; Kim, O.-K. *Polymer* **2000**, *41*, 5237.
(20) Liu, Y.-G.; Sui, Y.; Yin, J.; Gao, J.; Zhu, Z.-K.; Huang, D.-Y.; Wang, Z.-G. *J. Appl. Polym. Sci.* **2000**, *76*, 290.
(21) Lu, J.; Yin, J. *J. Polym. Sci., Part A: Polym. Chem.* **2003**, *41*, 303.
(22) Park, S. K.; Do, J. Y.; Ju, J. J.; Park, S.; Kim, M.; Lee, M.-H. *React. Funct. Polym.* **2006**, *66*, 974.
(23) Qiu, F.; Da, Z.; Yang, D.; Cao, G.; Li, P. *Dyes Pigm.* **2008**, *77*, 564.

(24) Sekkat, Z.; Wood, J.; Knoll, W.; Volksen, W.; Miller, R. D.; Knoesen, A. *J. Opt. Soc. Am. B* **1997**, *14*, 829.
(25) Chen, J. P.; Lagugne-Labarthet, F.; Natansohn, A.; Rochon, P. *Macromolecules* **1999**, *32*, 8572.
(26) Si, J.; Mitsuyu, T.; Ye, P.; Li, Zh.; Shen, Y.; Hirao, K. *Opt. Commun.* **1998**, *147*, 313.
(27) Meng, X.; Natansohn, A.; Rochon, P. *Polymer* **1997**, *38*, 2677.
(28) Sava, I.; Resmerita, A.-M.; Lisa, G.; Damian, V.; Hurduc, N. *Polymer* **2008**, *49*, 1475.
(29) Liu, Y. G.; Sui, Y.; Yian, J.; Gao, J.; Zhu, Z. K.; Huang, D.-Y.; Wang, Z.-G. *J. Appl. Polym. Sci.* **2000**, *76*, 290.
(30) Chen, T.-A.; Jen, A. K.-Y.; Cai, Y. *J. Am. Chem. Soc.* **1995**, *117*, 7295.
(31) Chen, T.; Jen, A.; Cai, Y. *Macromolecules* **1996**, *29*, 535.
(32) Schab-Balcerzak, E. *Pol. J. Chem.* **2008**, *82*, 2293.
(33) Ringsdorf, H.; Schmidt, H.-W. *Macromol. Chem.* **1984**, *185*, 1327.
(34) Sek, D.; Schab-Balcerzak, E.; Grabiec, E. *Polymer* **1998**, *39*, 7001.
(35) Chen, M.; Yu, L.; Dalton, L. R.; Shi, Y.; Steier, W. H. *Macromolecules* **1991**, *24*, 5421.
(36) Schab-Balcerzak, E.; Sobolewska, A.; Miniewicz, A. *Opt. Mater.* **2008**, *31*, 405.
(37) Bes, L.; Rousseau, A.; Mercier, R.; Sillion, B.; Toussaere, E. *High Perform. Polym.* **2000**, *12*, 169.
(38) Schab-Balcerzak, E.; Sek, D. *High Perform. Polym.* **2001**, *13*, 45.
(39) Ahlheim, M.; Lehr, F. *Macromol. Chem. Phys.* **1994**, *195*, 361.
(40) He, Y.; Yin, J.; Che, P.; Wang, X. *Eur. Polym. J.* **2006**, *42*, 292.
(41) Jiang, H.; Kakkar, A. K. *Macromolecules* **1998**, *31*, 4170.
(42) Cardoso, M. R. U.; Neves, M.; Misoguti, L.; Ye, Zh.; Bu, X. R.; Mendonca, C. R. *Opt. Mater.* **2006**, *28*, 1118.
(43) Wang, J.; Cao, W. F.; Su, J. H.; Tian, H.; Huang, Y. H.; Sun, Z. R. *Dyes Pigm.* **2003**, *57*, 171.
(44) Brown, D.; Natansohn, A.; Rochon, P. *Macromolecules* **1995**, *28*, 6116.
(45) Li, Z.; Zhao, Y.; Zhou, J.; Shen, Y. *Eur. Polym. J.* **2000**, *36*, 2417.
(46) Schab-Balcerzak, E.; Sobolewska, A.; Miniewicz, A.; Jurusik, J.; Jarzabek, B. *Polym. J.* **2007**, *39*, 659.
(47) Kim, D. Y.; Li, L.; Jiang, X. L.; Shivshankar, V.; Kumar, J.; Tripathy, S. K. *Macromolecules* **1995**, *28*, 8835.
(48) Tripathy, S. K.; Viswanathan, N. K.; Balasubramanian, S.; Bian, S.; Li, L.; Kumar, J. *NATO Sci. Ser., 3* **2000**, *79*, 421.
(49) Lagugné-Labarthet, F.; Buffeteau, T.; Sourisseau, C. *J. Phys. Chem. B* **1998**, *102*, 2654.
(50) Lagugné-Labarthet, F.; Buffeteau, T.; Sourisseau, C. *J. Phys. Chem. B* **1999**, *103*, 6690.
(51) Lagugné-Labarthet, F.; Buffeteau, T.; Sourisseau, C. *Appl. Phys. B* **2002**, *74*, 129.
(52) Fukuda, T.; Matsuda, H.; Shiraga, T.; Kimura, T.; Kato, M.; Viswanathan, N. K.; Kumar, J.; Tripathy, S. K. *Macromolecules* **2000**, *33*, 4220.
(53) He, Y.; Wang, X.; Zhou, Q. *Polymer* **2002**, *43*, 7325.
(54) Helgert, M.; Wenke, L.; Hvilsted, S.; Ramanujam, P. S. *Appl. Phys. B* **2001**, *72*, 429.
(55) Liu, W.; Lee, S. H.; Yang, S.; Bian, S.; Li, L.; Samuelson, L. A.; Kumar, J.; Tripathy, S. K. *J. Macromol. Sci., Pure Appl. Chem. A* **2001**, *38*, 1355.
(56) Sobolewska, A.; Miniewicz, A. *J. Phys. Chem. B* **2007**, *111*, 1536.
(57) Schab-Balcerzak, E.; Sobolewska, A.; Miniewicz, A.; Jurusik, J. *Polym. Eng. Sci.* **2008**, *48*, 1755.
(58) Grabiec, E.; Schab-Balcerzak, E.; Sek, D.; Sobolewska, A.; Miniewicz, A. *Thin Solid Films* **2004**, *453−454*, 367.
(59) Sobolewska, A.; Miniewicz, A.; Grabiec, E.; Sek, D. *Cent. Eur. J. Chem.* **2006**, *4*, 266.
(60) Strobl, G. R. *The Physics of Polymers*, 2nd ed.; Springer: New York, 1997; Chapter 5.

JP904250R